


RESEARCH ARTICLE

Drought Dynamics From Meteorological Stress to Agricultural Impacts Using Physically-Based Remote Sensing Indices in the Horn of Africa

Nasser A. M. Abdelrahim^{1,2,3}  | Shuanggen Jin^{4,5}

¹Shanghai Astronomical Observatory, Chinese Academy of Sciences, Shanghai, China | ²School of Astronomy and Space Science, University of Chinese Academy of Sciences, Beijing, China | ³Civil Engineering Department, Faculty of Engineering, Sohag University, Sohag, Egypt | ⁴School of Artificial Intelligence, Anhui University, Hefei, China | ⁵School of Surveying and Land Information Engineering, Henan Polytechnic University, Jiaozuo, China

Correspondence: Shuanggen Jin (sgjin@hpu.edu.cn; sg.jin@yahoo.com)

Received: 9 April 2025 | **Revised:** 24 October 2025 | **Accepted:** 29 October 2025

Funding: This work was supported by the Henan International Science and Technology Cooperation Key Project (grant no. 24111520700), Henan Department of Education's 'Double First-Class' Project (grant no. 760507/033) and Henan Polytechnic University Startup Foundation Project (grant no. 722403/067/002).

Keywords: agricultural | DPI | drought propagation | Horn of Africa | meteorological

ABSTRACT

Drought significantly affects agriculture and ecology in the Horn of Africa (HOA), whereby livelihoods largely depend on rainfed farming. This study aims to analyze drought propagation and its impacts on vegetation and crop productivity, with a specific focus on recovery dynamics. Over the period 2000–2022, we developed and integrated a suite of physically based remote sensing indices, including the Drought Propagation Index (DPI), Crop Stress Index (CSI), Soil Moisture Deficit (SMD), Water Deficit Index (WDI), and Drought Recovery and Rate Index (DRRI), into a novel framework. The performance of this integrated framework was further evaluated against the conventional Standardised Precipitation Index (SPI) to validate its ability for capturing drought propagation and agricultural impacts. The findings identify the eastern and southeastern HOA as major drought hot-spots, experiencing severe droughts 70%–100% of the time and exhibiting worsening temporal trends. SPI was strongly correlated with DPI ($r=0.67$, $p<0.05$), thus proving to be reliable. Vegetation indices showed significant reductions during droughts, while DPI positively correlated with NDVI at 0.56 and EVI at 0.54. Crop production was reduced by 30%–35% in Somalia, especially for maize and sorghum, whereas Ethiopia showed more resistance because of irrigation. The mean recovery time exceeded 2 months during the 2010 and 2016 droughts in southeastern HOA, indicating low resilience, whereas northern areas recovered faster. This framework offers practical recommendations for drought mitigation, drought-resistant crops, and adaptive resource management to deal with vulnerabilities.

1 | Introduction

Accurate drought monitoring is fundamental for effective drought risk assessment and for minimising agricultural losses (Abdelrahim and Jin 2025a; Alasow et al. 2024; Edokossi et al. 2024; Elameen et al. 2023; Jin et al. 2024; Jin and Zhang 2016; Wen et al. 2023). Since the 1970s, drought events have become more severe,

prolonged, and widespread, resulting in longer drought durations and more catastrophic outcomes than previous droughts (Kafy et al. 2023; Mwangi et al. 2013; Todmal 2024). A deficit in precipitation is the primary cause of drought, which propagates through the hydrological cycle and manifests as meteorological, hydrological, agricultural, and socioeconomic types (Abdelrahim and Jin 2025b; Bilal and Gupta 2024; Khan et al. 2021; Masih et al. 2014; Wu

et al. 2019). Due to its complex interactions with soil, crops, and climate, agricultural drought is both one of the most critical and least investigated types of drought (Abdelrahim and Jin 2025c; Guiqin et al. 2012; Liu et al. 2016; Wilhelmi and Wilhite 2002). Agricultural drought directly threatens food security, emphasising the urgent need to enhance drought early warning systems (Kogan et al. 2019; Naumann, Barbosa, et al. 2014; Naumann, Dutra, et al. 2014). Meteorological drought is frequently considered a prelude to other types of droughts, and there is generally a high correlation between it and other forms of drought (Li et al. 2020; Ogunrinde et al. 2024; Xu et al. 2023). The transition from one drought type to another is referred to as 'drought propagation', and it is commonly characterised by a spatiotemporal lag between meteorological and agricultural manifestations. Analysis of drought propagation is crucial for creating robust drought-resistant plans (Chaulagain et al. 2025; Ma et al. 2025; Ning et al. 2025; You et al. 2025; Faiz et al. 2023; Inocencio et al. 2021; Xu et al. 2021). Soil moisture dynamics, irrigation practices, and vegetation resilience strongly influence drought propagation (Han et al. 2019; Xu et al. 2021).

The Horn of Africa (HOA) is the eastern region of Africa, which includes countries such as Ethiopia, Eritrea, Somalia, and Djibouti. The majority of the population resides in rural areas and depends predominantly on subsistence farming (Adloff et al. 2022; Qu et al. 2019). In order to comprehend and describe extreme phenomena such as droughts, extensive research has been conducted in the HOA over the past decade (Nguvava and Abiodun 2023). Due to the scarcity of observational data across the region (Agutu et al. 2021), the majority of these studies have relied on simulated data. Limited analysis of drought transmission from climatic to agricultural drought has resulted from the lack of observational data, particularly on soil moisture and crop performance (Odongo et al. 2023). Although numerous studies have examined drought propagation from meteorological or hydrological to agricultural domains (Bhardwaj et al. 2020; Das et al. 2023, 2022; Ding et al. 2021; Fawen et al. 2023; Gevaert et al. 2018; Han et al. 2019; Jehanzaib et al. 2020; Ma et al. 2023; Zhou et al. 2024), relatively few studies examine how drought spreads in the HOA, particularly from meteorological to agricultural. For instance, Odongo et al. (2023) conducted basin-scale analysis in the HOA using SPI, SSMI, and SSI to examine meteorological-to-soil-moisture and meteorological-to-streamflow propagation using correlation analysis and duration ratios in 318 catchments. They were interested in catchment-scale hydrological propagation and did not model vegetation or crop stress. Xu et al. (2021) provided a long-term climatology of SPI-SSI propagation in China using copula models and found that propagation probabilities are generally higher in humid regions. However, their study was restricted to country-level meteorological-soil drought interactions and did not address the recovery stages of agricultural drought. Han et al. (2019) investigated groundwater-drought propagation in the Pearl River Basin using GRACE and GLDAS data to analyze water-storage and climatic forcing parameters. The study illustrates delayed drought propagation (up to 8 months) and large-scale oscillations' influence but does not include surface-level vegetation or soil-crop processes.

With a particular focus on long-term drought evaluations over the HOA, Gebremeskel Haile et al. (2020) investigated the regional

and chronological trends in drought duration, frequency, and intensity. Qu et al. (2019) used precipitation data collected from the Tropical Rainfall Measuring Mission (TRMM) and remotely sensed satellite products from the Moderate Resolution Imaging Spectroradiometer (MODIS) to study severe drought in the HOA region. However, the mechanisms governing the propagation of meteorological drought into agricultural systems remain unclear, even though numerous characteristics have been investigated for drought assessment and early-warning purposes (Xu et al. 2021). This indicates that meteorological-to-agricultural drought propagation has not yet been well researched, despite the significance of food security and livelihood implications for the HOA. This represents a critical research gap that warrants urgent scientific and policy-oriented attention. Addressing this gap is essential for developing integrated drought monitoring and response strategies by considering the interconnectedness of meteorological patterns and agricultural productivity in the region (Li et al. 2020; Zhou et al. 2024).

While previous studies have examined the propagation of drought from meteorological to hydrological or agricultural forms (Abera et al. 2020; Agutu et al. 2020; Amazirh et al. 2023; Gebremeskel Haile et al. 2020; Han et al. 2022; Odongo et al. 2023; Xu et al. 2021), few have offered an integrated assessment of the full cascade, from meteorological stress through soil moisture deficits to agricultural impact and vegetation recovery, especially in data-scarce, semi-arid regions like the HOA.

Unlike prior studies focusing primarily on single indices or specific drought types, this framework holistically examines the cascading effects of meteorological drought on soil moisture (Alasow et al. 2024; Gevaert et al. 2018), vegetation health (Rossi et al. 2023), and crop production (Guga et al. 2023; Venkatappa et al. 2021), including the time-lagged responses (Jeong et al. 2024; Wu et al. 2024) of agricultural systems (Xu et al. 2021). This study introduces a Drought Propagation Index (DPI), integrating five synergistic indices (SPI, SMD, CSI, WDI, and DRRI) to diagnose not only the onset and peak but also the spatial and temporal transition and recovery phases of drought. By validating DPI against SPI, NDVI, EVI, and FAO crop data, the study offers a robust tool to quantify drought severity and recovery, providing actionable insights for resilience-building strategies. This multi-dimensional approach advances the understanding of drought impacts and fills critical gaps in early warning systems for drought-prone regions like the HOA (Bhardwaj et al. 2020).

The key scientific questions addressed in the framework of this study are: How does drought propagate from meteorological conditions to agricultural systems, and what are the impacts on crop health in the HOA? Considering drought propagation, what is happening with respect to crop production? How do physically based parameters improve our understanding? How can we quantify the time lag between drought onset and its effects on vegetation and crop health? The main goal of this study is to formulate a physically based model for drought propagation and recovery, which integrates key meteorological and agricultural parameters. The current study, therefore, anticipates an improvement in the accuracy and interpretability of the drought monitoring system by accounting for the physical mechanisms underlying drought dynamics: soil moisture balance,

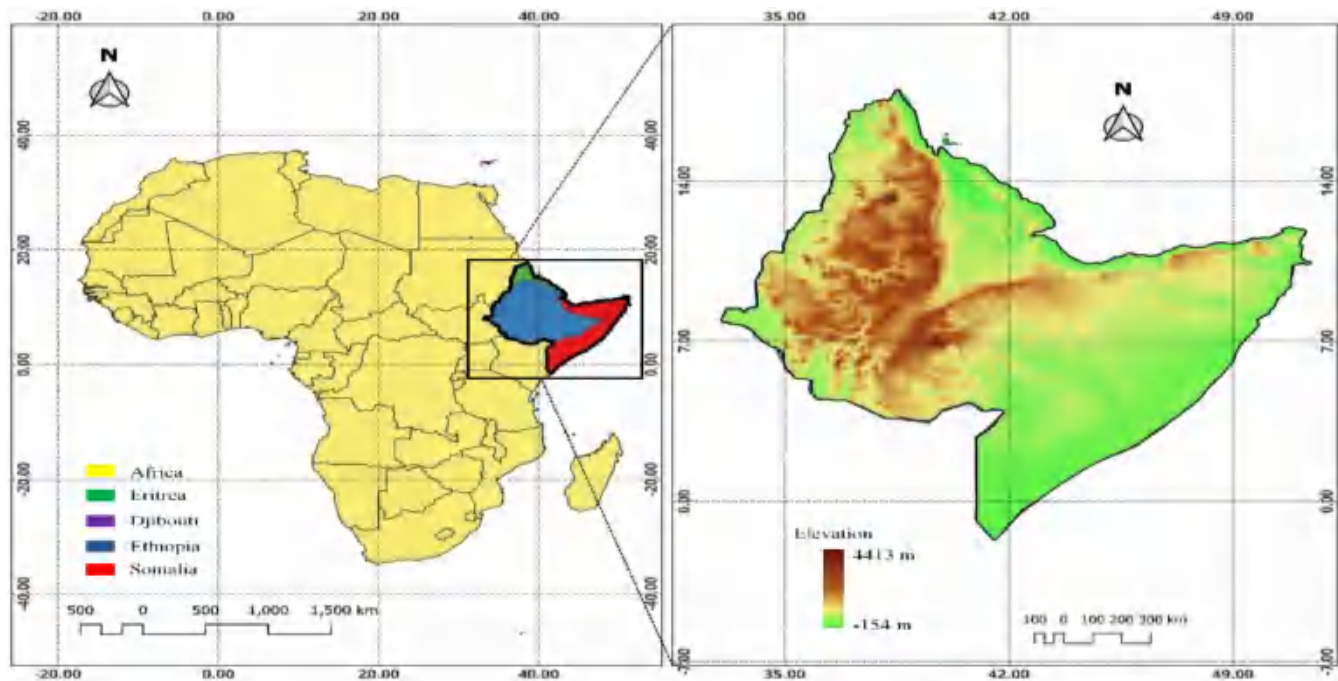


FIGURE 1 | Study area map of the Horn of Africa. The map highlights the four countries analysed (Eritrea, Ethiopia, Somalia, and Djibouti), spanning from 2.1°S to 17.55°N and from 33.17°E to 51.48°E. Elevation ranges from −154 m to 4413 m. The region is characterised by arid to semi-arid climates, diverse topography, and reliance on rainfed agriculture. [Colour figure can be viewed at [wileyonlinelibrary.com](https://onlinelibrary.wiley.com)]

evapotranspiration, crop water requirements, and vegetation health. Some of the specific objectives of this study are outlined as follows: (1) To develop an integrated modelling framework representing drought propagation from meteorological to agricultural impacts, considering the soil moisture, crop stress, and energy balance components. (2) To derive physically based parameters, including WDI, DRRI, CSI, and DPI, that capture drought severity and recovery at a high spatial and temporal scale. (3) To assess the drought impact on the health and production of crops within the HOA region with particular emphasis on maize, sorghum, and wheat crops. (4) To validate the model using observed crop production data from FAO. The remainder of this paper is organised as follows: Section 2 describes the materials and methods, Section 3 presents the results and related discussions, and Section 4 concludes the study.

2 | Materials and Methods

2.1 | Study Areas

HOA comprises predominantly arid and semi-arid areas, as well as some highly arid regions, making it one of the world's most drought-prone zones. Drought constitutes the predominant environmental hazard in the region, with far-reaching consequences including food insecurity, socioeconomic instability, and disruptions to livelihoods (Han et al. 2022). The study area encompasses Eritrea, Ethiopia, Somalia, and Djibouti (Leal Filho et al. 2022), as shown at Figure 1. This region represents a wide range of climates, topographies, and vegetation types (Abdelrahim and Jin 2025d; Abera et al. 2020). Geographically, HOA extends from 2.1°S to 17.55°N and 33.17°E to 51.48°E, covering approximately 1.88 million km². The countries included in this study were selected because of their recent experiences with severe drought

events and recurrent food security crises, which have resulted in significant human and livestock losses. Major droughts struck Somalia from 2011 to 2013 and again in 2017 (Epule et al. 2024).

Eritrea exhibits both arid and temperate climates, receiving 200–600 mm of rainfall annually, most of which falls over the highlands and sustains crops such as millet and sorghum (Joordens et al. 2019; Tierney et al. 2015). Ethiopia ranges from arid lowlands to high plateaus exceeding 4400 m (Beyene et al. 2023). Rainfall varies from ≈200 mm in dry zones to over 1200 mm in fertile highlands, where crops such as maize, sorghum, and coffee are cultivated. Somalia is primarily arid to semi-arid, receiving 100–500 mm of highly variable annual rainfall. Most of its crops, such as bananas and maize, are produced along the river basins (Measho et al. 2020; Warsame et al. 2021). In contrast, Djibouti has an arid desert climate with rainfall below 200 mm and very little agriculture, except for small-scale vegetable and date production on extremely limited arable land. These countries face significant problems, including water scarcity, erratic rainfall, and reliance on rainfed agriculture, which impact food security and economic stability (Afuecheta and Omar 2021; Alasow et al. 2024; Epule et al. 2024; Han et al. 2022; Qu et al. 2019). Table 1 summarises the climatic properties for each country in the study area.

2.2 | Datasets

2.2.1 | Standardised Precipitation-Evapotranspiration Index (SPEI)

The SPEI was obtained from the SPEIbase v2.9 dataset developed by the Spanish National Research Council (CSIC) and provides a widely recognised drought index that considers precipitation and potential evapotranspiration. It quantifies drought severity by

TABLE 1 | Climatic properties of the Horn of Africa countries.

Country	Precipitation (mm/year)	Elevation (m)	Temperature range (°C)	Main crops	Climate type
Eritrea	200–600	–75 to +3018	15–40	Sorghum, wheat	Arid to temperate, with wetter highlands
Ethiopia	200–1200+	–125 to +4413	10–40	Coffee, maize, sorghum	Arid, semi-arid, and temperate highlands
Somalia	100–500	–0.5 to +2416	20–45	Maize, sorghum, sesame	Arid to semi-arid, riverine areas more humid
Djibouti	< 200	–154 to +2028	25–45	Dates, vegetables	Arid desert with extreme heat

Note: Summarizes annual precipitation, elevation ranges, temperature range, dominant crops, and climate types for Eritrea, Ethiopia, Somalia, and Djibouti.

calculating water-balance anomalies across multiple time scales. The dataset has high temporal resolution, thus providing insight into the variability of water deficits in the short and long term. SPEI (3-month scale) is especially effective for reflecting climatic extremes and trends, hence suitable for the analysis of drought in arid and semi-arid regions like HOA (Dong et al. 2023; Vicente-Serrano et al. 2010).

2.2.2 | CHIRPS Precipitation Dataset

The CHIRPS dataset provides daily precipitation data at a spatial resolution of 0.05°, combining satellite imagery with in situ station observations to generate accurate rainfall estimates across diverse terrains. This dataset is particularly valuable in regions with sparse meteorological networks, such as large parts of the HOA.

CHIRPS data have been instrumental in monitoring rainfall anomalies, evaluating drought onsets, and calculating indices such as SPI (Bhardwaj et al. 2020; Li 2024; Mehravar et al. 2021; Naumann, Barbosa, et al. 2014; Naumann, Dutra, et al. 2014; Rincón-Avalos et al. 2022; Wu et al. 2019).

2.2.3 | Actual Evapotranspiration (AET) – FAO WaPOR

The FAO/WaPOR dataset uses satellite-derived information and advanced energy balance models to provide Actual Evapotranspiration (AET). AET quantifies actual water loss from the Earth's surface and vegetation; hence, it is considered a fundamental component in assessing water availability and drought stress (Elnashar et al. 2021; Senay et al. 2022; Xu et al. 2023).

2.2.4 | ERA5-Land Reanalysis—PET, Soil Moisture, and Runoff

ERA5-Land provides high-resolution estimates of potential evapotranspiration (PET), representing the atmospheric demand for water. These estimates integrate temperature, humidity, and radiation data, offering valuable inputs for drought analysis (Hao et al. 2022; Jury 2023; Li et al. 2022; Xiang et al. 2020; Zomer et al. 2022).

ERA5-Land soil moisture data reflect volumetric water content within the root zone (0–100 cm), representing the fraction of soil

water accessible for plant uptake. This dataset offers high spatial and temporal resolution, allowing for detailed studies of water stress on crops. Root-zone moisture is critical in agricultural drought analysis, as it reflects the accessibility of water to vegetation. Incorporating root-zone soil moisture in drought propagation models strengthens the quantified link between climatic anomalies and agricultural impacts (Li et al. 2022; Mahmood et al. 2024; Sahaar and Niemann 2024).

ERA5-Land runoff data quantify surface and subsurface water flow, providing critical information for hydrological drought studies and facilitating the evaluation of water availability and resource sustainability in river basins. Runoff metrics further support the assessment of meteorological drought impacts on hydrological systems (Ho et al. 2021).

2.2.5 | Vegetation Indices—MODIS NDVI and EVI

The MODIS/006/MOD13Q1 dataset delivers satellite-derived vegetation indices, including Normalised Difference Vegetation Index (NDVI) and Enhanced Vegetation Index (EVI). Both indices are proxies of vegetation health and greenness. Vegetation health proxies are critical for monitoring agricultural and ecological droughts. This dataset covers seasonal and interannual variability of vegetation dynamics at 250-m resolution and with 16-day compositing periods. NDVI and EVI have been widely applied to assess drought impacts on crop productivity and vegetation stress (Nguyen et al. 2023; Zhen et al. 2023).

2.2.6 | Soil Moisture—NASA GLDAS

The NASA/GLDAS dataset provides surface zone soil moisture data, which tracks water content in the upper soil layers. This dataset is crucial for understanding the initial impacts of meteorological drought on soil conditions and vegetation. It aids agricultural planning by identifying areas prone to water stress (Han et al. 2019; Mohseni et al. 2024; Sazib et al. 2018).

2.2.7 | Standardised Precipitation Index (SPI)

The Standardised Precipitation Index (SPI) was calculated directly from CHIRPS precipitation data, which provides daily

TABLE 2 | Datasets used for drought propagation analysis. Details sources, spatial/temporal resolutions, and applications of datasets.

Dataset	Source	Resolution	Temporal frequency	Key applications
SPEI	CSIC SPEIbase	~0.5°	Monthly	Multi-scalar drought monitoring.
Precipitation (CHIRPS)	UCSB	0.05° (~5.5 km)	Daily	Drought monitoring, water resource management.
Actual evapotranspiration	FAO WaPOR	100–250 m	Monthly	Crop water productivity, irrigation planning.
Potential evapotranspiration	ECMWF ERA5-Land	0.1° (~11 km)	Monthly	Water balance calculations, drought monitoring.
Root-zone soil moisture	ECMWF ERA5-Land	0.1° (~11 km)	Monthly	Agricultural drought evaluation.
Surface soil moisture	NASA GLDAS	0.25° (~27 km)	Monthly	Soil moisture analysis.
NDVI/EVI	MODIS MOD13Q1	250 m	16 days	Vegetation health monitoring.
Runoff	ECMWF ERA5-Land	0.1° (~11 km)	Monthly	Hydrological drought assessment.
Crop production	FAO	—	Annual	Validation of agricultural drought indices.
SPI	Derived (CHIRPS)	0.05° (~5.5 km)	Monthly	Meteorological drought detection.

precipitation values at a high spatial resolution of 0.05°. This index standardises precipitation anomalies over specified timescales, making it a fundamental metric for evaluating meteorological drought conditions. By relying on long-term precipitation records, SPI quantifies deviations from typical rainfall patterns and identifies periods of drought severity and intensity in the Horn of Africa (Li et al. 2022; Sakellariou et al. 2024). SPI was also employed to validate drought-propagation timing, as it is optimised for long-term agricultural drought assessment.

2.2.8 | FAO Crop Production Data

The Food and Agriculture Organization (FAO) crop production dataset provides detailed statistics on crop yields, harvested area, and production volume. National-level annual crop production data for maize, sorghum, and wheat were obtained from FAOSTAT for Ethiopia, Somalia, and Eritrea. For each country and crop, production anomalies were computed by subtracting the long-term (2000–2022) mean from each year's value. This enabled comparison with aggregated drought indices on a consistent basis while accounting for interannual variation.

Validating drought models with empirical data, particularly those linked to agricultural impacts, is essential. By linking climatic and soil variables with crop outputs, this dataset enables the evaluation of the economic and food security implications of drought (FAO 2022, 2021, 2019).

All remote sensing and reanalysis datasets used in this study were accessed and processed through the Google Earth Engine (GEE) platform, which provides cloud-scalable geospatial analysis solutions (Mullissa et al. 2021; Pan et al. 2023). These steps allowed for smooth integration of the datasets, reducing biases due to different resolutions and ensuring that the metrics were robust

and comparable for drought analysis (Agutu et al. 2021; Rossi et al. 2023; Yao 2022). All data details are summarised at Table 2.

2.3 | Methods

As illustrated at Figure 2, the methodology focuses on developing and applying a physically based drought propagation and recovery model that integrates key meteorological, hydrological, and agricultural parameters to assess drought impacts on crop production across the HOA.

The model utilises high-resolution climate, soil moisture, and vegetation data for estimating drought severity and recovery in agro-systems. All datasets span the period 2000–2022 and collectively represent the drought-susceptible environment of the HOA.

The GEE platform, Python scripts, and Geographic Information Systems (GIS) software were employed to download, process, and analyze these datasets.

2.3.1 | Data Preprocessing

Given the contrasting temporal and spatial resolutions of the datasets—CHIRPS (0.05°), GLDAS (0.25°), ERA5-Land (0.1°), and MODIS (250 m)—a harmonisation procedure was implemented to ensure cross-compatibility and minimise aggregation errors. All datasets were resampled to a common 0.05° grid. Continuous variables, including precipitation, soil moisture, and PET, were resampled using bilinear interpolation to preserve gradient continuity (Addesso et al. 2017; Bussalleu et al. 2024; Iman Bin Hussain et al. 2025; Pastick et al. 2018). MODIS NDVI and EVI products were first quality-screened and then aggregated to 0.05° by mean compositing, thereby retaining sub-pixel

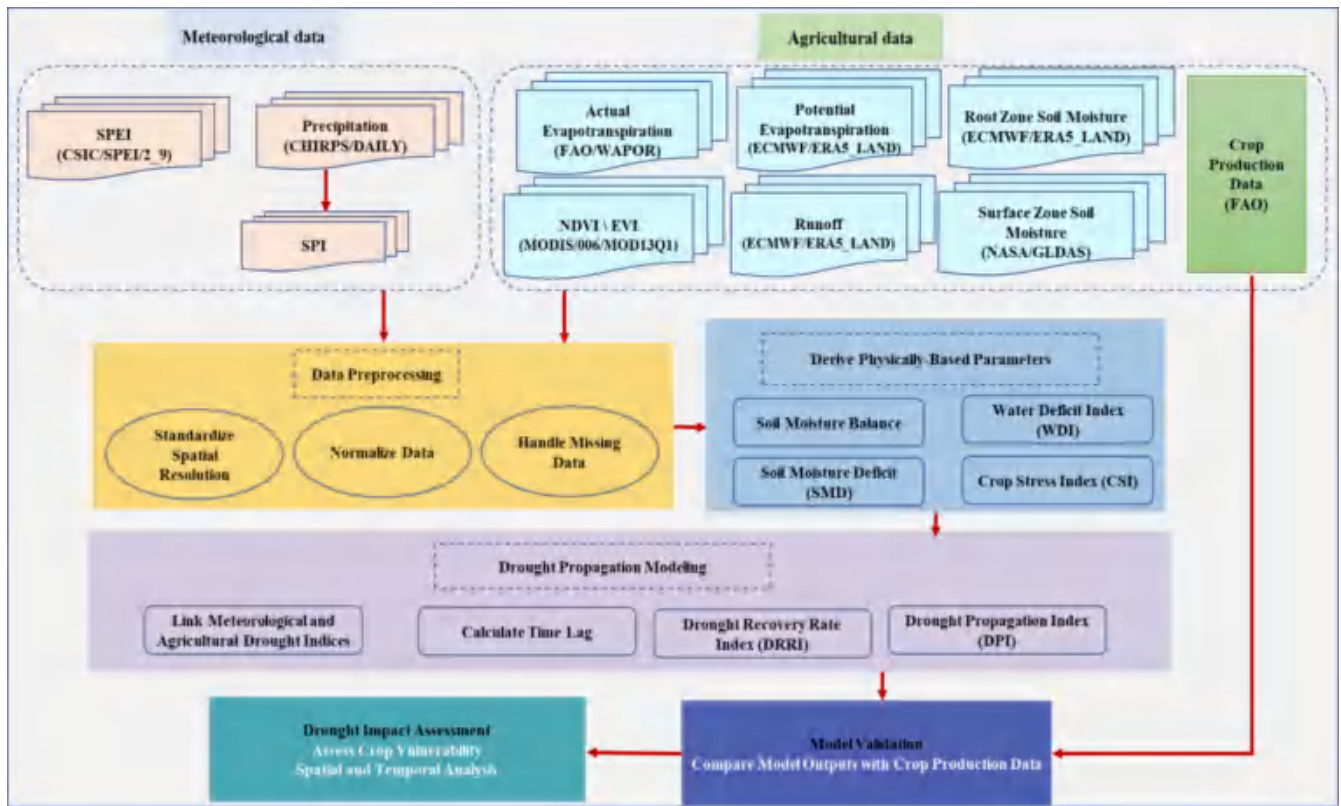


FIGURE 2 | Workflow of the integrated drought propagation framework. [Colour figure can be viewed at [wileyonlinelibrary.com](https://onlinelibrary.wiley.com/doi/10.1002/joc.70178)]

variability. Temporal harmonisation involved bringing all datasets to a monthly timestep. CHIRPS daily rainfall values were summed to monthly totals, while MODIS 16-day composites were converted to a monthly series using the maximum value composite (MVC) method to limit the influence of cloud cover. Reanalysis GLDAS and ERA5-Land variables were aggregated to monthly averages. Quantile mapping was also applied to correct systematic biases in the reanalysis products, using CHIRPS and MODIS as standards of reference. The cumulative distribution functions (CDFs) of variables were synchronised on a monthly, pixel-wise basis, thereby incorporating both central tendency and higher-order moments of data (Farrag et al. 2020; Bhatti et al. 2016; García et al. 2016; Ouattiki et al. 2023; Pandey et al. 2017; Yaswanth et al. 2023; Zhang et al. 2022).

2.3.2 | Physically-Based Parameters

The methodology focuses on deriving physically based parameters that represent the critical processes of drought propagation and recovery. To estimate soil-water storage (Equation 1), the soil moisture balance model was applied (Cao 2022). The model incorporates precipitation, evapotranspiration, and runoff to estimate soil moisture content at each time step.

$$\text{Soil moisture}_t = \text{Soil moisture}_{t-1} + \text{Precipitation}_t - \text{Evapotranspiration}_t - \text{Runoff}_t \quad (1)$$

This model estimates soil-water availability for crops and forms the basis for evaluating drought stress within

agricultural systems. Subsequently, the soil-water deficit was computed to assess available water under the input-output balance governing crop growth. Further, WDI, as shown at Equation (2), is calculated in order to quantify crop water stress (Cagatay et al. 2017). This index uses AET and PET to determine the amount of water available to crops and helps in evaluating water stress at different stages of crop development. It has proven effective for tracking crop-water stress and assessing water availability under drought conditions (Ahmad et al. 2021; Cagatay et al. 2017). Positive WDI values indicate surplus water, where AET exceeds PET—conditions often linked to waterlogging or excessive irrigation. However, negative WDI values indicate water stress, where crops cannot transpire at their potential rate due to limited availability of water. Near-zero WDI values represent the optimum for plant growth, as water demand is fully met.

$$\text{WDI} = \frac{\text{AET}}{\text{PET}} - 1 \quad (2)$$

The Soil Moisture Deficit (SMD) represents the shortage of soil moisture compared to its field capacity and therefore indicates locations suffering from drought stress under inadequate water supply conditions.

If the soil moisture is below field capacity, plants suffer from water stress, and growth and productivity are reduced. When soil moisture exceeds field capacity, the SMD is set to zero because surplus water does not further alleviate crop stress. To improve SMD estimation accuracy, spatially variable field-capacity (θ_{fc}) and wilting-point (θ_{wp}) values were derived

from the SoilGrids v2.0 global database (De Sousa et al. 2020; Hengl et al. 2017; Poggio et al. 2021). SoilGrids provides high-resolution (250 m) machine learning predictions of soil hydraulic properties from global soil profile data. For each pixel, θ_{fc} and θ_{wp} were derived by averaging the upper 0–60 cm layer and extrapolating values to 100 cm depth. The SMD was then calculated as the positive difference between field capacity and ERA5-Land root-zone soil moisture (0–100 cm) (Equation 3), allowing spatial consistency in water stress appraisal across various soil textures.

$$SMD(x, y, t) = \max(0, \theta_{fc}(x, y) - \theta_{SM}(x, y, t)) \quad (3)$$

where θ_{SM} is the ERA5-Land root-zone soil-moisture content (0–100 cm) and $\theta_{fc}(x, y)$ is the soil-specific field capacity derived from SoilGrids.

The Crop Stress Index (CSI) evaluates the stress experienced by crops due to insufficient water in the root zone relative to their water requirements (Equation 4).

$$CSI = \min\left(2, \frac{\text{Root} - \text{Zone Soil Moisture}}{\text{Crop Water RequirementRoot}}\right) \quad (4)$$

Root-Zone Soil Moisture represents the available soil moisture in the crop root zone, typically 0–60 cm depth, derived from ERA5-Land data. This zone is critical because it is where plants draw water and nutrients. Crop Water Requirement (CWR), or the amount of water needed to balance evapotranspiration loss, was calculated from reference evapotranspiration (ET_0) and crop coefficients (K_c) according to FAO-56 guidelines (Equation 5) (Shao et al. 2021), with regional modifications for crops such as maize, sorghum, and wheat.

$$CWR_{(i,t)} = K_{c(i,s)} \cdot ET_{0(t)} \quad (5)$$

where $K_{c(i,s)}$ denotes the crop-specific coefficient for growth stage $s \in \{\text{initial, development, mid-season, late season}\}$, and $ET_{0(t)}$ is the reference evapotranspiration at time t , derived from ERA5-Land using the FAO Penman–Monteith equation. Crop calendars were obtained from FAO-GIEWS and national reports and adjusted for interannual variability through smoothed NDVI peaks to determine phenological changes. The K_c values applied were maize (0.3–1.2), sorghum (0.4–0.95), and wheat (0.35–1.15), adjusted seasonally according to each crop's phenological stages across the Horn of Africa. CSI was computed on a monthly basis using dynamic CWR values rather than static annual means to be sensitive to water stress seasonally.

The CSI expresses the degree to which root-zone moisture satisfies a crop's water demand. Values near or above 1 suggest no water stress exists, whereas values below 1 do. An upper cap of 2 is applied to limit CSI and ensure that excess moisture beyond twice the crop demand does not disproportionately inflate the composite DPI. Empirical analyses across multiple growing seasons showed that CSI values exceeding 2 correspond to persistently wet conditions, where additional moisture fails to increase yield and may induce adverse hydraulic effects (Akuraju et al. 2021; Alordzinu et al. 2021; Katimbo et al. 2022).

The Drought Recovery Rate Index (DRRI) quantifies the speed at which soil moisture and vegetation indices recover after a drought. It is calculated by measuring the change in soil moisture or NDVI/EVI before and after a drought event, as shown at Equation (6). This index reflects the resilience of agricultural systems to recover from drought stress and provides insights into the duration required for recovery (Ge et al. 2025; Yao 2022).

$$DRRI = \frac{\Delta \text{NDVI}}{\Delta \text{Time}} \quad (6)$$

2.3.3 | Drought Propagation Modelling

Drought propagation describes the sequential process by which precipitation deficits (meteorological drought) lead to reductions in streamflow and groundwater availability (hydrological drought), ultimately depleting soil moisture and imposing stress on crops (agricultural drought), with distinct time lags separating each impact stage (Zhou et al. 2024). To model this process, meteorological drought indices such as SPEI are linked to agricultural drought indicators including SMD and CSI. The time lag between drought onset and its impact on soil moisture and vegetation is calculated by using cross-correlation methods (Nigatu et al. 2024). The statistical significance of lag correlations was confirmed using a t-test, and only significant correlations ($p < 0.05$) were retained. Autocorrelation in the time series was addressed by pre-whitening prior to cross-correlation analysis to minimize spurious relationships. These methods help determine the delay between meteorological droughts and their subsequent effects on agricultural systems. This step is necessary to understand the process by which droughts propagate through different systems and over what time frame the soil moisture and crops will reach a critical level of stress. Cross-correlation is a statistical technique used to examine the similarity between two time series as a function of the lag applied to one of them, as shown at Equation (7). This approach is widely applied in hydrology, meteorology, and environmental studies to assess the temporal relationships between variables (Li et al. 2024; Vicente-Serrano et al. 2010; Wei et al. 2023).

$$R_{xy}(k) = \frac{\sum_t (x_t - \bar{x})(y_{t+k} - \bar{y})}{\sqrt{\sum_t (x_t - \bar{x})^2 \sum_t (y_{t+k} - \bar{y})^2}} \quad (7)$$

where $R_{xy}(k)$ is the cross-correlation coefficient at lag k ; x_t is the value of the first time series (e.g., SPEI) at time t ; y_{t+k} is the value of the second time series (e.g., SMD or CSI) at time $t+k$ (lagged by k time steps); \bar{x} and \bar{y} are the respective means of the two series; and k represents the lag (in time steps) applied to the second series.

The DPI is a novel composite metric developed in this study, integrating lag-adjusted agricultural drought indices (SMD and CSI) weighted by SPEI. Its formulation, depicted in Equation (8), captures the cascading effects of meteorological droughts on agricultural systems by quantifying how meteorological anomalies propagate through soil-moisture depletion and vegetation stress.

$$DPI = \text{SPEI}_{\text{weight}, x, y} * \left(\frac{\overline{SMD}_{x, y}}{\overline{SMD}_{x, y}} + \frac{\overline{CSI}_{x, y}}{\overline{CSI}_{x, y}} \right) \quad (8)$$

where $\overline{\text{SMD}}_{x,y}$ and $\overline{\text{CSI}}_{x,y}$ are the mean annual values of SMD and CSI, respectively, at pixel (x, y) for a given year, and $\text{SMD}_{x,y}$ and $\text{CSI}_{x,y}$ are the respective lag times (in months) obtained from statistically significant correlations ($p < 0.05$). $\text{SPEI}_{\text{weight},x,y}$ is the normalised absolute SPEI, capturing the intensity of meteorological drought and calculated as shown at Equation (9).

$$\text{SPEI}_{\text{weight},x,y} = \frac{|\text{SPEI}_{x,y}| - \min(|\text{SPEI}|)}{\max(|\text{SPEI}|) - \min(|\text{SPEI}|)} \quad (9)$$

SPEI data were derived from the SPEIbase v2.9 dataset (Vicente-Serrano et al. 2010), which applies a log-logistic distribution to monthly climatic water-balance data (precipitation minus PET). We used the 3-month aggregation (SPEI-3), given its relevance to short- and medium-term agricultural drought impacts.

To achieve comparability across regions and time, DPI values were min–max normalized to the range [0,1] over the whole spatiotemporal extent. Pixels with non-significant lag correlations ($p \geq 0.05$) were masked when calculating DPI to reduce uncertainty. Consequently, the resulting index captures both the rate and magnitude of drought propagation in a physically interpretable and statistically robust way.

Drought-intensity frequency was determined by categorising monthly DPI values into severity classes: extreme ($\text{DPI} < 0.2$), severe ($0.2 \leq \text{DPI} < 0.4$), moderate ($0.4 \leq \text{DPI} < 0.6$), mild ($0.6 \leq \text{DPI} < 0.8$), and no drought ($\text{DPI} \geq 0.8$). Annual frequencies were derived by counting months within each class, following SPI-based drought classification (Vicente-Serrano et al. 2010).

Although indices such as the Vegetation Condition Index (VCI) and Scaled Drought Condition Index (SDCI) (Wei et al. 2021) are effective for monitoring specific drought phases, they neglect the sequential and lagged propagation dynamics that DPI explicitly incorporates. By consolidating SPI, SMD, and CSI into a temporally sensitive framework, DPI facilitates improved monitoring and early warning of drought impacts in data-scarce, agriculturally sensitive regions such as the Horn of Africa.

2.3.4 | Model Validation

Validation of the DPI was performed through rigorous statistical testing to ensure its reliability for agricultural drought assessment. Temporal correlations between DPI and SPI were quantified using Pearson's correlation coefficient (Shen et al. 2019). Comparison of DPI against SPI enabled evaluation of the model's ability to capture the propagation of drought impacts from meteorological to agricultural systems. This comparison verified that DPI effectively incorporates climatic anomalies and translates them into meaningful indicators of soil moisture and vegetation stress. Furthermore, validating DPI against crop-production data provides insights into its practical relevance for agricultural monitoring and management. Crop production metrics, obtained from datasets

such as FAO, serve as direct indicators of agricultural performance under drought conditions (Bhanja et al. 2016; Shen et al. 2019). Because FAO crop-production data are reported at the national level, DPI values were aggregated over cropland areas within each country to enable consistent-scale comparisons. The resulting time series were compared with national crop-yield anomalies for maize, sorghum, and wheat to assess the coherence between observed production changes and remotely sensed drought stress.

Assessment of drought effects on crop health and productivity involved analysing relationships between DPI and vegetation indices (e.g., NDVI, EVI) and examining spatial DPI patterns across regions with different crop types and water requirements. This analysis enables identification of drought-vulnerable areas and crop types, thereby informing adaptive agricultural management practices (Sardooi et al. 2021).

3 | Results and Discussion

3.1 | Water Deficit Index (WDI) Variations

The spatial and temporal variations of WDI across the study area from 2000 to 2022 reveal pronounced fluctuations in water-stress conditions, as illustrated at Figure 3. The results indicate distinct seasonal and interannual patterns of water availability and deficit. Across all years, January consistently shows low WDI values (near or below -1) in the northern and central regions, indicating heightened water stress driven by limited precipitation and reduced evapotranspiration recovery during the dry season. May and August show a gradual improvement in WDI values, with larger regions displaying positive or near-zero values, particularly in the southern and eastern areas. This reflects increased precipitation and water availability during the growing season. In November, WDI values decline again, particularly in central and western regions, marking the transition to the dry season and the depletion of soil-moisture reserves.

The years 2000 and 2005 exhibit widespread negative WDI values across most of the region, especially during the dry seasons, indicating prolonged drought conditions and significant water stress for crops. The year 2015 shows a resurgence of heightened water stress in the northern regions, with persistent negative WDI values across all months, corresponding to a period of severe drought. The northern highlands consistently experience greater water stress compared to the southern and eastern regions. This is attributed to lower precipitation and higher evapotranspiration demands. Conversely, the southern regions display more positive WDI values during May and August, reflecting better water availability during the rainy season.

3.2 | Soil Moisture Deficit (SMD)

High SMD values indicate substantial deficits in soil moisture, signifying insufficient water to meet crop-water requirements. Such conditions impose severe stress on crops, often resulting in yield reduction or crop failure. Conversely, low SMD values indicate adequate or surplus soil moisture, favorable for crop growth and indicating successful replenishment of soil water reserves.

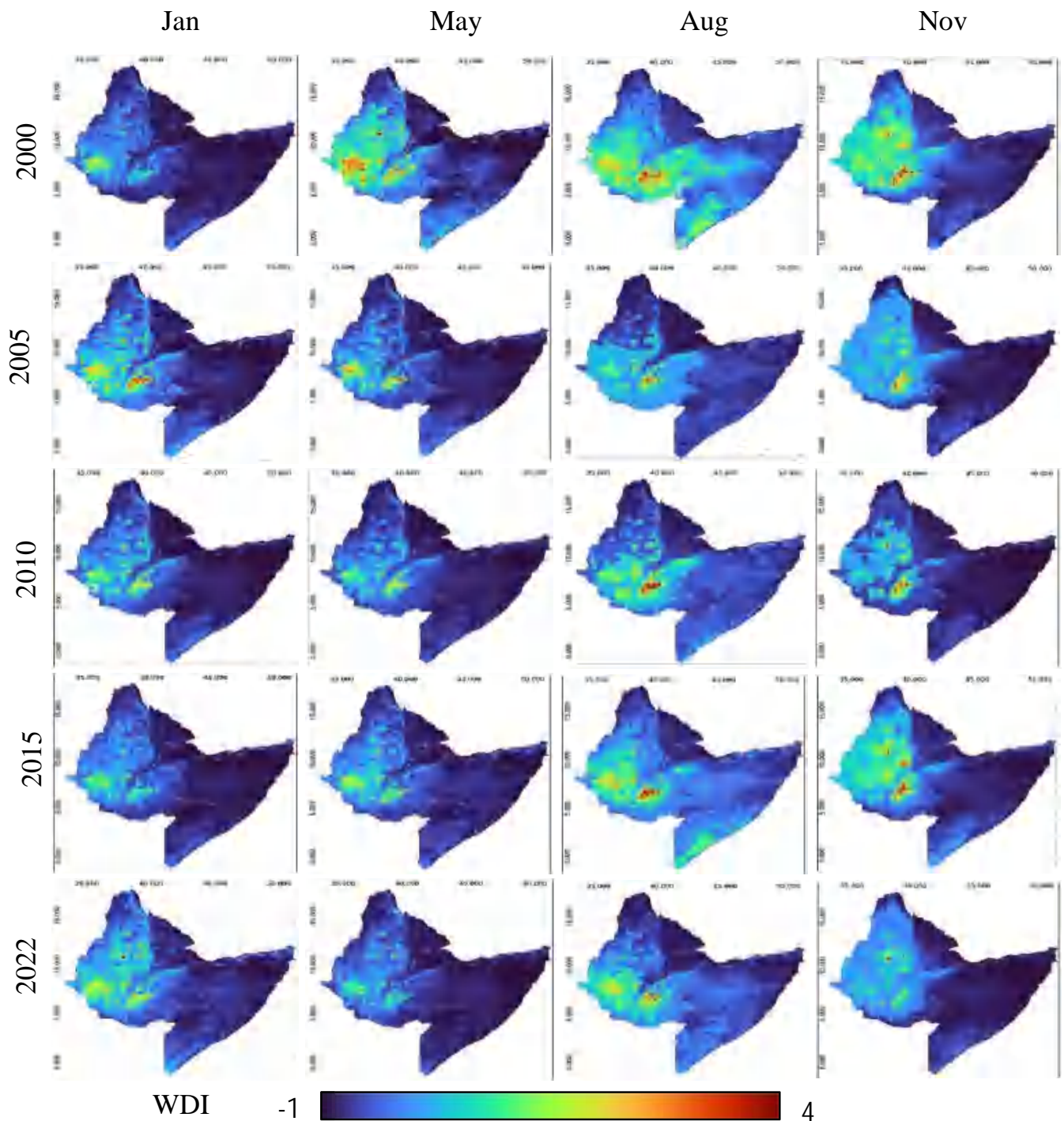


FIGURE 3 | Spatiotemporal variation of the Water Deficit Index (WDI) across the HOA (2000–2022). WDI quantifies crop water stress (negative values) or surplus (positive values). [Colour figure can be viewed at [wileyonlinelibrary.com](https://onlinelibrary.wiley.com/doi/10.1002/joc.70178)]

The highest SMD values, corresponding to severe moisture deficits, occur during the dry months (e.g., January), particularly across the northern and central regions, as shown at Figure 4. These values indicate low soil moisture availability relative to crop water demands during periods of reduced precipitation. During wetter months, such as May, lower SMD values appear in many areas, reflecting replenished soil moisture due to increased rainfall. However, regions in the northern highlands still exhibit moderate to high deficits, suggesting persistent aridity. The years 2000 and 2005 are characterised by widespread high SMD

values, indicating significant soil moisture shortages throughout the region. This pattern aligns with historical records of severe droughts during these years. The year 2013 exhibits noticeable improvement in soil moisture availability across portions of the southern and eastern regions during the wet season, although the central and northern areas continued to experience moderate deficits. In 2022, mixed conditions were observed, with localised areas of low SMD values in the south but persistent deficits in the northern and central zones, suggesting partial recovery yet continued vulnerability to water stress.

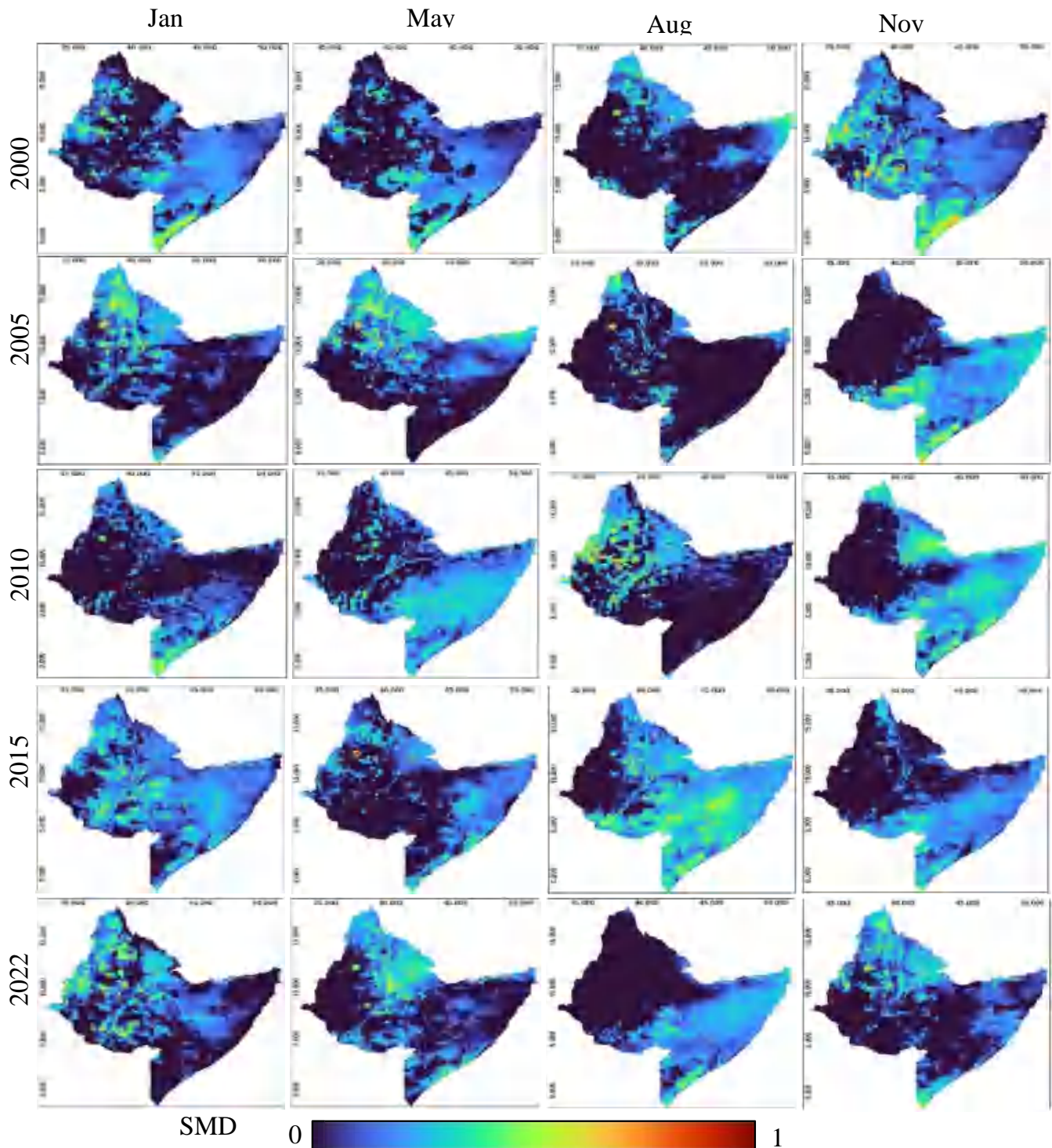


FIGURE 4 | Soil Moisture Deficit (SMD) dynamics in the HOA (2000–2022). SMD reflects soil moisture shortages relative to field capacity. Northern and central regions face severe deficits (> 45 mm) during dry months (January), with Ethiopia's highlands showing resilience due to irrigation. Somalia's arid zones exhibit prolonged deficits. [Colour figure can be viewed at [wileyonlinelibrary.com](https://onlinelibrary.wiley.com/doi/10.1002/joc.70178)]

The southern regions exhibit comparatively lower SMD values, particularly during wet months, due to greater rainfall and enhanced soil-water retention. The southern regions exhibit comparatively lower SMD values, especially during wet months, due to higher rainfall and better water retention in soils. Central agricultural zones show pronounced interannual variability in

SMD, reflecting their dependence on seasonal rainfall and consequent vulnerability to drought.

Furthermore, all WDI and SMD maps represent monthly averages, offering a consistent temporal snapshot of hydrological conditions throughout the study period. Cumulative

values or specific event-based analyses are explicitly noted where applicable.

3.3 | Crop Stress Index

The spatial and temporal distribution of the Crop Stress Index (CSI) illustrates how root-zone soil moisture and crop-water requirements vary over time and space, providing valuable insights into crop-water stress under different environmental conditions. Figure 5 shows that during dry months, CSI values are generally high across most areas, particularly in the northern and central regions. This indicates pronounced water stress, since the soil moisture available in the root zone is less than the amount required by crops. During the wet months, lower CSI values are observed, signifying reduced water stress due to increased soil-moisture availability; however, some arid zones still experience stress because of limited moisture retention capacity.

The years 2000 and 2004 exhibit widespread elevated CSI values, consistent with known drought years. These elevated values reflect substantial water stress that adversely affected agricultural productivity during those years. In 2013, notable improvement is observed, with lower CSI values primarily in the southern regions, indicating reduced water stress.

However, the central and northern zones still have moderate stress levels, highlighting uneven recovery. In 2015, CSI values increased again, indicating intensified crop-water stress associated with another severe drought event. In 2022, spatial heterogeneity is evident: southern areas display lower CSI values, while northern regions remain high, reflecting unequal water availability and crop stress across the landscape. These spatial contrasts underscore the heterogeneous distribution of water availability and crop stress across the study area.

3.4 | Time Lag

The time lag in CSI illustrates the delayed response of plants and ecosystems to drought-induced stress. Figure 6 presents the spatial and temporal variability of drought-response times across the study area. Short response lags (0–2 months) are mostly seen in northern, central, and southern Ethiopia during years when droughts are likely (like 2002, 2005, 2011, and 2015). These areas, depicted as dark to light blue zones, represent ecosystems that are either weakly buffered or respond rapidly to rainfall deficits, particularly regions dominated by annual crops or sparse vegetation. The farming systems of the central highlands respond rapidly, illustrating how quickly water stress manifests in crop health. Long response lags (8–11 months) are found in the eastern lowlands, including the Somali and Afar regions, and some parts of the western and southern highlands. In these areas, the ecosystem has a slow response time. Either perennial plants or rangelands respond over longer periods to stress due to the moisture stored in the soil or because deep-rooted plants are affected later. Areas exhibiting short response lags (blue zones) are more sensitive to rapid drought impacts and may require timely interventions to mitigate agricultural losses. Conversely, regions with longer response lags underscore the importance of

monitoring delayed drought impacts on ecosystems dependent on subsurface moisture reserves.

The time lag for SMD illustrates the number of months it takes for soil moisture to deplete once a meteorological drought sets in, as shown at Figure 7. This measure characterises the progression of hydrological drought and the soil's capacity to withstand rainfall deficits. Short response times (0–2 months) are common in farming areas of the central and northern highlands, as well as some parts of southern Ethiopia. These areas, coloured in dark to light blue, are defined by thin soils and large water extraction by crops; thus, the soil moisture depletes rapidly once rainfall is below normal. The Rift Valley also exhibits short lags, indicating limited soil-water storage capacity. Long response lags (8–11 months) occur in the eastern and southeastern lowlands, such as the Somali and Afar regions, where delayed responses are depicted as dark red zones.

This suggests the presence of deeper soil profiles or reliance on subsurface water sources, which slow the rate of soil-moisture depletion. Western Ethiopia, especially the forested areas, has a consistently long lag, indicating that vegetation cover is denser and thus water loss is slower. Areas with short lags are highly susceptible to immediate drought impacts and require improved water-retention strategies such as mulching, terracing, or enhanced irrigation practices. Longer response lags in areas such as the eastern lowlands indicate delayed soil-water depletion, which may, however, mask latent vulnerabilities if drought conditions persist. The short CSI lags generally fall in the same regions as short SMD lags, especially in the central highlands and northern Ethiopia.

This pattern indicates rapid vegetation and soil responses to meteorological drought, reflecting high vulnerability in these regions. Conversely, combinations of long SMD lags and short CSI lags, observed in the eastern lowlands, indicate ecosystems exhibiting immediate stress responses without concurrent soil-moisture depletion, likely influenced by vegetation type or soil depth. The eastern lowlands consistently show longer lags for both metrics, again highlighting the resilience of the rangelands and natural vegetation to drought conditions. However, if drought conditions persist, these regions may require extended periods for ecological recovery. In contrast, agricultural zones in the highlands display shorter lags, reflecting the immediate impacts of drought on highly water-dependent cropping systems sensitive to rainfall variability. Figure 8 illustrates the mean time lag for both CSI and SMD.

3.5 | DPI Variations

The spatial and temporal analysis of the DPI over the period 2000–2022 reveals pronounced spatial heterogeneity and interannual variability in drought conditions, as illustrated at Figure 9. Areas with consistently high DPI values, indicating severe drought susceptibility, are prominently concentrated in specific regions throughout the study period. Temporal patterns indicate substantial interannual variation, with notable intensification during 2004, 2014, and 2018, corresponding to major regional drought events. Conversely, years like 2001 and

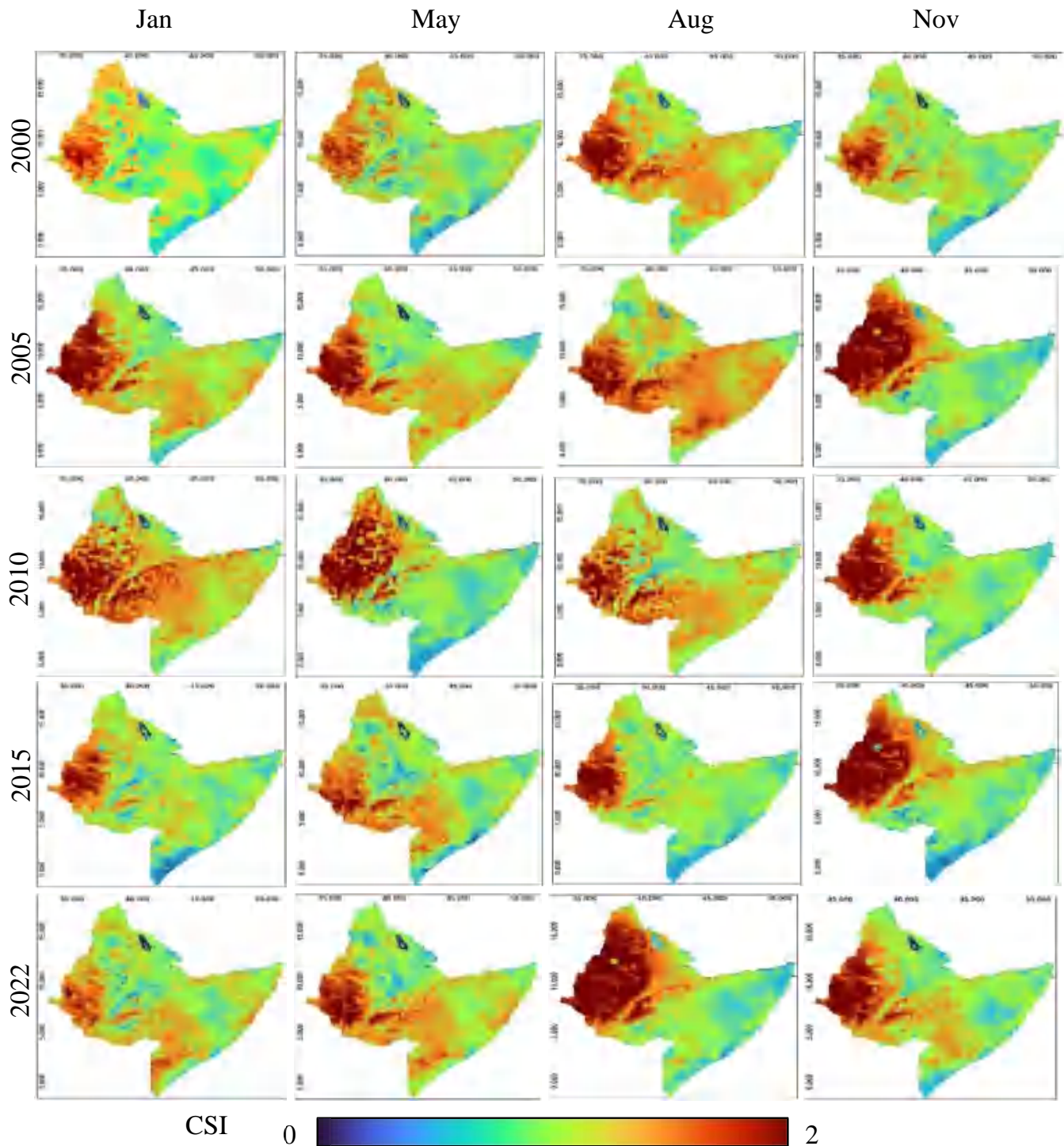


FIGURE 5 | Crop Stress Index (CSI) spatial and temporal patterns (2000–2022). CSI measures root-zone moisture adequacy for crops. Values < 1 indicate stress. Northern and central HOA show elevated stress during droughts (2000, 2005). Southern regions recover partially in wet seasons but remain vulnerable in dry months. [Colour figure can be viewed at [wileyonlinelibrary.com](https://onlinelibrary.wiley.com/doi/10.1002/joc.70178)]

2013 exhibit relatively lower DPI values, indicating periods of reduced drought impact. Spatially, the northern and eastern regions are more prone to recurrent drought conditions, as evidenced by persistently high DPI values. These observed patterns align with established climatic variability and may reflect the influence of global phenomena such as El Niño and La Niña events, which modulate drought intensity and frequency in the region.

3.6 | Validation of DPI

Validation of the DPI using SPI, SPEI, and crop-yield data reaffirms its robustness as a drought-monitoring tool and its suitability for assessing crop impacts. The Pearson correlation between SPI and DPI was 0.67 ($p < 0.05$) over the study period (Figure 10a), indicating a significant positive relationship consistent with findings from previous studies in arid and semi-arid environments. To

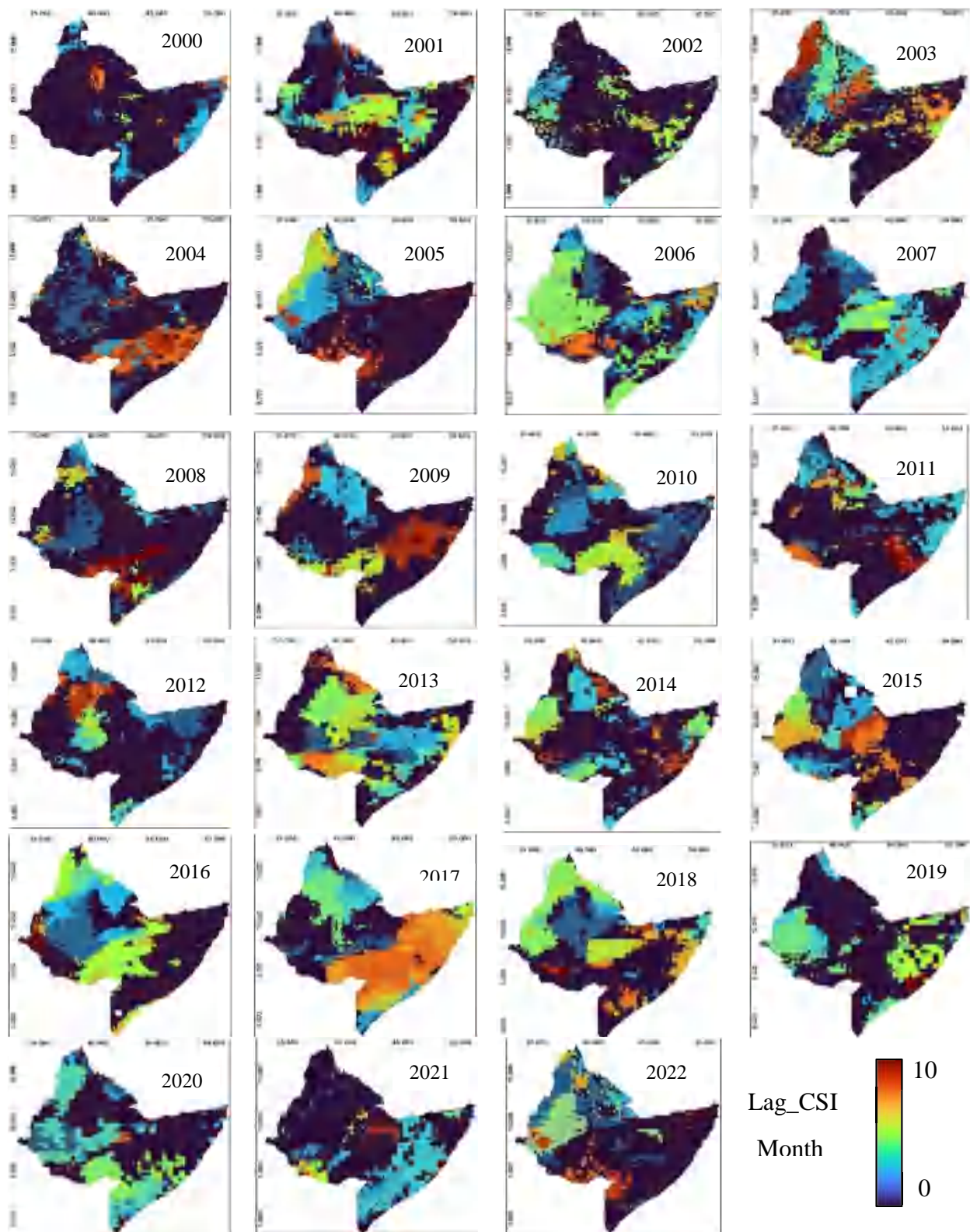


FIGURE 6 | Time lag (months) between meteorological drought onset and Crop Stress Index (CSI) response. Short lags (0–2 months, dark blue) in Ethiopia's highlands reflect rapid crop stress, while eastern lowlands (Somalia/Afar) show delayed responses (8–11 months, dark red) due to deeper soils or perennial vegetation. [Colour figure can be viewed at [wileyonlinelibrary.com](https://onlinelibrary.wiley.com/doi/10.1002/joc.70178)]

further evaluate model performance, the Root Mean Square Error (RMSE) and Mean Bias Error (MBE) were calculated between DPI and other indices (SPI, SPEI, and NDVI). The outcomes at the four major drought years (2011, 2014, 2016, and 2018) showed that DPI

had a lower RMSE and was less biased than SPI and SPEI, particularly during the peak drought periods (Table 3). In addition, DPI showed higher concordance with NDVI anomalies in areas of crop production, detecting vegetation stress and lagged drought

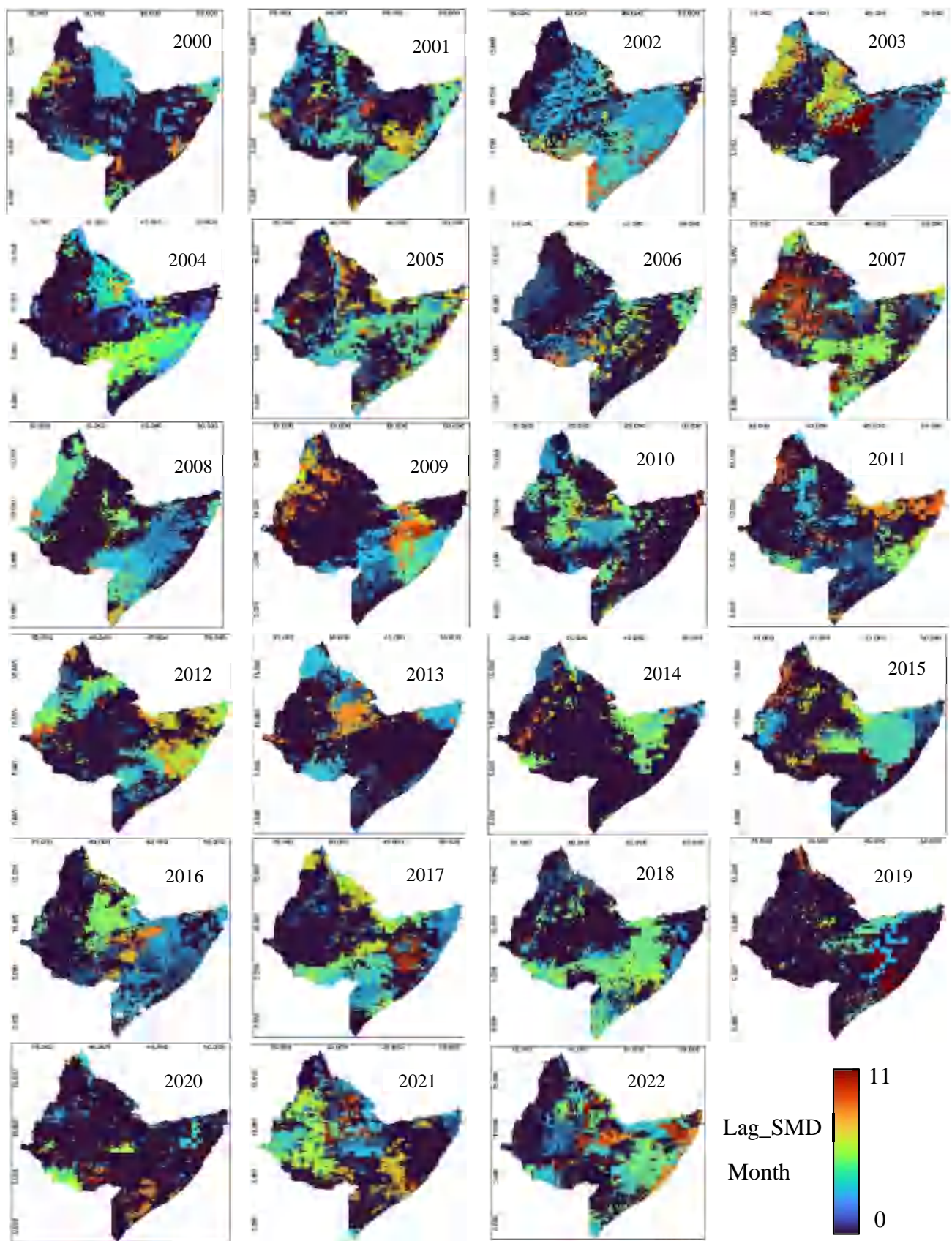


FIGURE 7 | Time lag (months) for Soil Moisture Deficit (SMD) after drought onset. Northern highlands and Rift Valley exhibit rapid depletion (0–2 months), whereas eastern lowlands retain moisture longer (8–11 months). Reflects soil type and agricultural practices influencing drought propagation. [Colour figure can be viewed at [wileyonlinelibrary.com](https://onlinelibrary.wiley.com)]

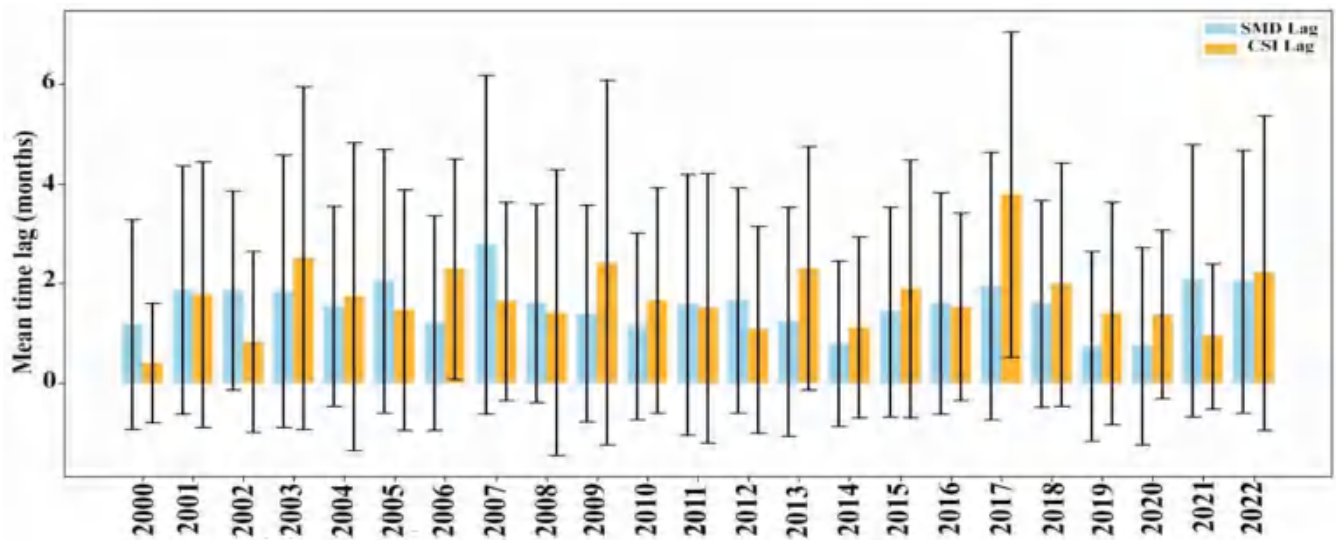


FIGURE 8 | Mean time lag (months) for CSI and SMD (2000–2022). Highlights regional variability: Northern Ethiopia (0–2 months) versus Somali lowlands (8–11 months). Critical for tailoring early warnings to agroecological zones. Error bars indicate the standard deviation of lag times across spatial grid cells, reflecting spatial variability in drought propagation dynamics. [Colour figure can be viewed at [wileyonlinelibrary.com](https://onlinelibrary.wiley.com/doi/10.1002/joc.70178)]

effects better than precipitation indices alone. Further, the performance of DPI was evaluated against regional crop production data for major crops, including maize, sorghum, and wheat. The analysis showed a clear inverse relationship between crop yields and DPI values in drought years, as illustrated at Figure 10b. To test the equivalence of simulated drought stress and measured agricultural production, we related yearly DPI measurements to standardised crop yield anomalies (z -scores) for three principal crops: maize, sorghum, and wheat. Standardisation removed between-crops unit variation by expressing annual production in units of standard deviations of the long-term average. The composite yield anomaly was the average z -score of the three crops each year.

As shown at Figure 10b, negative yield anomalies tend to occur coincidentally with years of low DPI, such as 2014, 2016, and 2018. The correlation between DPI and mean crop anomaly was $r = 0.61$ ($p < 0.05$), suggesting DPI captures general patterns of agricultural stress consistent with documented yield deviations. Nevertheless, this correlation should not be interpreted as causal, since other confounding variables (e.g., market shocks, pests, or conflict) were not controlled in this study. The objective is to demonstrate the indicative capacity of DPI to detect potential yield losses, rather than to attribute declines in production solely to drought. A low value of the same corresponds to a sharp decline in crop production, which indicates agricultural outputs are sensitive to drought stress. This is reflected in the inverse relationship between peaks in DPI and troughs in crop production, especially for the drought-sensitive crops of maize and sorghum. Maize and sorghum indeed are the most responsive crops in the negative direction to drought stress, as reflected by abrupt falls in their production during high DPI years such as 2004, 2014, and 2016. These crops are highly dependent on adequate soil moisture, and their production is slower to recover after drought years. Rice and sugarcane production appeared less directly affected by DPI fluctuations. This may be due to the irrigation systems used for rice and sugarcane, which cushion the impact of drought. This validation confirms DPI as a robust tool bridging meteorological drought indices and agricultural

outcomes, providing a holistic framework for drought monitoring and impact mitigation.

The ability of DPI to successfully detect agricultural drought conditions was also evaluated based on its performance during severe drought years of the past decades in the Horn of Africa, such as the record droughts of 2014 and 2016. During these events, DPI values declined sharply, accurately delineating the spatial extent and magnitude of agricultural stress. Comparisons with SPI, SPEI, and NDVI during these events revealed that, while all indices indicated drought conditions, DPI most effectively captured the direct and cascading impacts on agricultural systems, closely aligning with reported crop losses and food-insecurity patterns. For example, during the 2011 drought, DPI values declined drastically throughout the impacted areas, indicating serious soil moisture deficits and crop stress, and were supported by independent accounts of extensive agricultural losses. This highlights the added value of DPI in detecting and characterising agricultural drought events more effectively than single-parameter indices.

However, the relationship should be viewed as associative rather than causal, since potential confounding factors (e.g., market shocks, pest outbreaks, or conflict) were not controlled in this analysis. The purpose here is to establish evidence of the indicative value of DPI for detection of possible yield loss, but not assign declines in production to drought alone.

3.7 | DPI Variations

Spatial variations in drought hotspots and temporal trends in the DPI from 2000 to 2022 reveal substantial spatial disparity across the Horn of Africa. The left panel (Figure 11a) illustrates the percentage of area affected by severe droughts, ranging from 0% (no drought) to 100% (persistent severe drought) during the study period. The right panel (Figure 11b) presents the temporal DPI trends between 2000 and 2022, ranging from -1 (strong

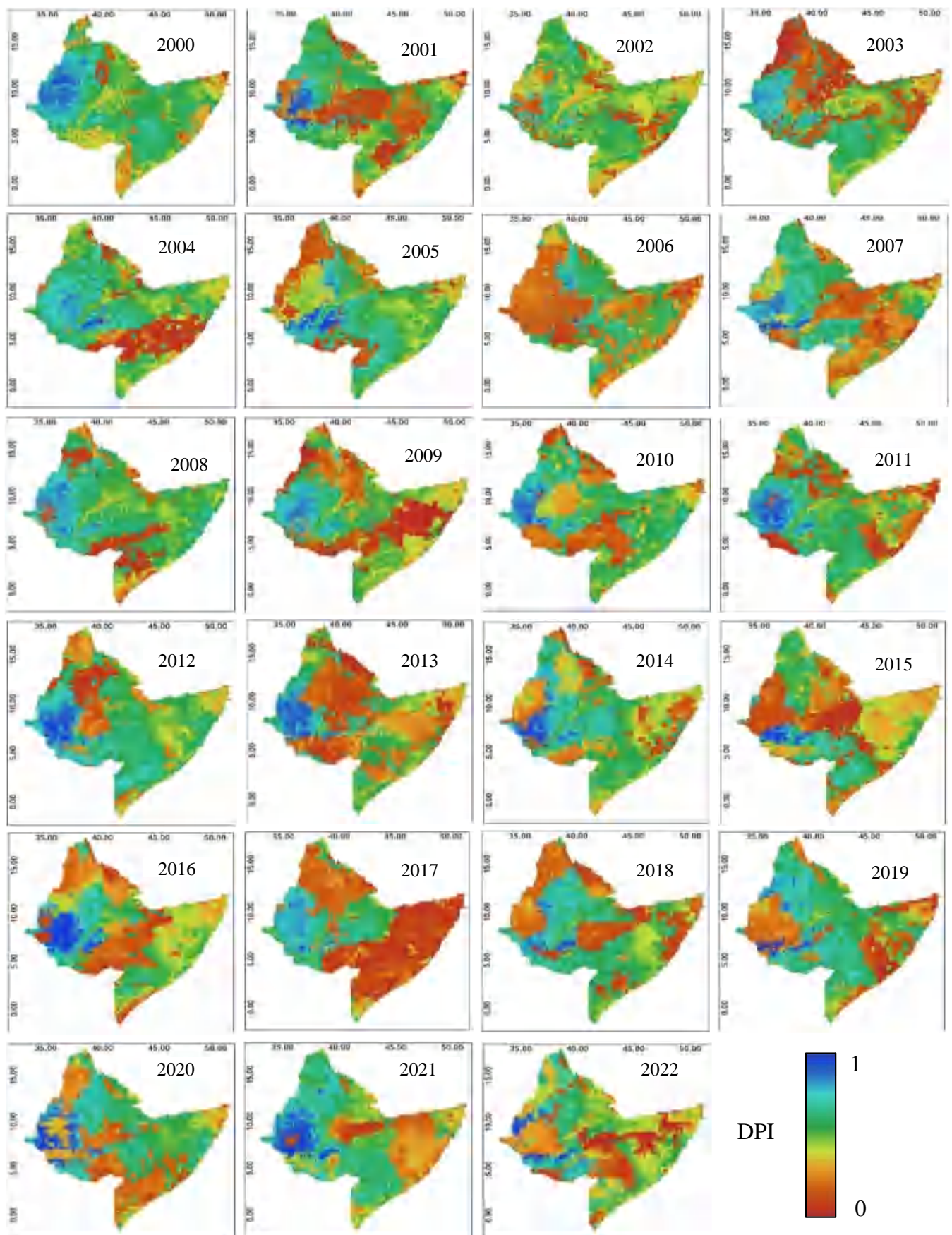


FIGURE 9 | Drought Propagation Index (DPI) spatiotemporal trends (2000–2022). DPI integrates SPEI, SMD, and CSI to quantify cascading drought impacts. Eastern/southeastern HOA are hotspots (DPI < 0.4, severe drought), with intensification during El Niño/La Niña events (e.g., 2010, 2018). [Colour figure can be viewed at [wileyonlinelibrary.com](https://onlinelibrary.wiley.com/doi/10.1002/joc.70178)]

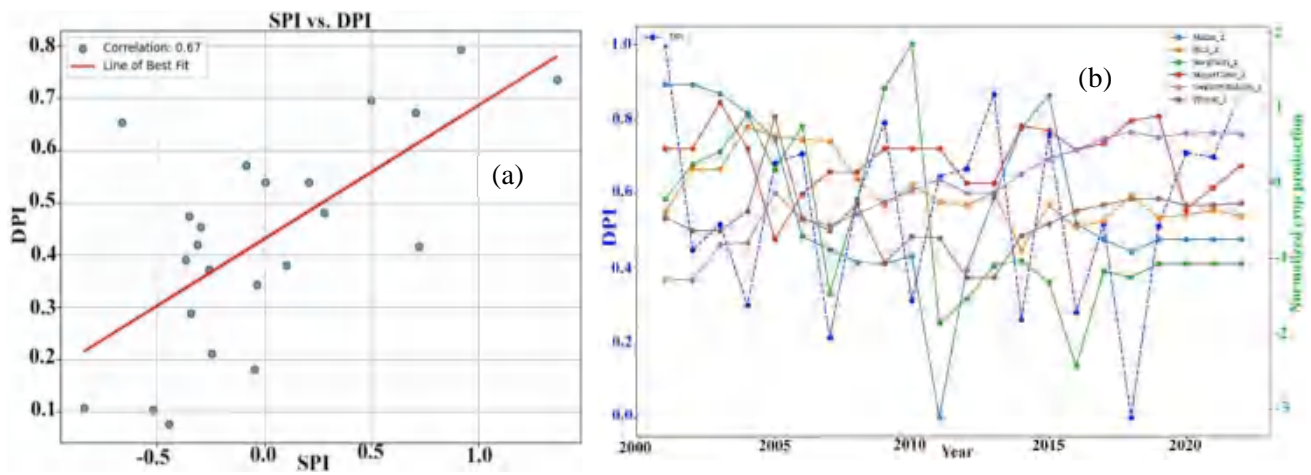


FIGURE 10 | Validation of DPI against SPI and crop production. (a) Strong correlation ($r=0.67$, $p<0.05$) between DPI and SPI confirms meteorological-agricultural drought linkage. (b) Inverse relationship between DPI and maize/sorghum yields in Somalia, highlighting rainfed vulnerability. [Colour figure can be viewed at [wileyonlinelibrary.com](https://onlinelibrary.wiley.com)]

TABLE 3 | Statistical comparison of DPI with SPI, SPEI, and NDVI during major drought years (2009, 2011, 2016, 2020) across HOA.

Compared		r (Correlation)	RMSE	MBE
Year	index			
2011	SPI	0.78	0.17	-0.05
	SPEI	0.80	0.15	-0.03
	NDVI	0.56	0.21	+0.06
2014	SPI	0.76	0.18	-0.06
	SPEI	0.81	0.14	-0.02
	NDVI	0.61	0.25	+0.07
2016	SPI	0.70	0.22	-0.10
	SPEI	0.74	0.19	-0.07
	NDVI	0.57	0.20	+0.05
2018	SPI	0.68	0.19	-0.09
	SPEI	0.72	0.17	-0.06
	NDVI	0.54	0.22	+0.08

negative trend) to +1 (strong positive trend). Negative trends denote worsening drought conditions, whereas positive values indicate improving precipitation and moisture conditions over time. Accordingly, the eastern and southeastern regions emerge as the most critical drought hotspots, exhibiting a high frequency of severe droughts (70%–100%) combined with strongly negative DPI trends, indicating intensifying drought conditions. Low precipitation, poor soil-moisture retention, and heavy dependence on rainfed agriculture render these regions particularly vulnerable to climatic variability. In contrast, northern and northwestern areas have lower frequencies of drought in the range of 0%–40%, with positive trends in DPI, which indicates that the precipitation conditions are improving over time with reduced drought severity. Central regions display heterogeneous patterns, with localized areas showing both worsening and improving trends.

These findings underscore the urgency of prioritizing drought mitigation strategies in the most affected regions while leveraging improving conditions in less vulnerable areas to enhance resilience and promote sustainable resource management.

3.8 | Impact of Drought on Vegetation Health and Crop Production

A moderate positive correlation between DPI and EVI can be seen at Figure 12a with a Pearson's correlation coefficient of 0.54. This indicates that higher DPI values (reflecting less intense drought) correspond to better vegetation health, as represented by higher EVI values. Since EVI is sensitive to the structure and biomass of the vegetation canopy, it shows that long-term drought stress reduces vegetation productivity and biomass accumulation. Similarly, a moderate positive correlation ($r=0.56$) was recorded between DPI and NDVI (Figure 12b).

NDVI primarily reflects vegetation greenness and photosynthetic activity, indicating that drought conditions generally suppress photosynthetic vigor. As the value of DPI increases, vegetation recovers and becomes healthier, reflected in improved NDVI values. Both the mean and maximum NDVI values (Figure 12c) show interannual variation that closely matches changes in the DPI. During major drought years—2002, 2007, 2011, and 2014—NDVI values declined markedly, indicating reduced vegetation greenness and photosynthetic activity due to water stress. Conversely, NDVI values recover during years with higher DPI, reflecting vegetation resilience and favorable growing conditions during wetter periods. Temporal EVI trends follow those of NDVI, with both mean and maximum EVI values (Figure 12c) decreasing during drought years. However, the impact of drought is slightly more pronounced on EVI than on NDVI, probably as a consequence of the sensitivity of EVI to changes in canopy structure and biomass. This suggests that drought impacts extend beyond photosynthetic activity (as captured by NDVI) to affect the structural and productive capacity of vegetation. These results emphasize the need for drought mitigation strategies to maintain vegetation health, particularly given the expected rise in drought frequency due to climate change.

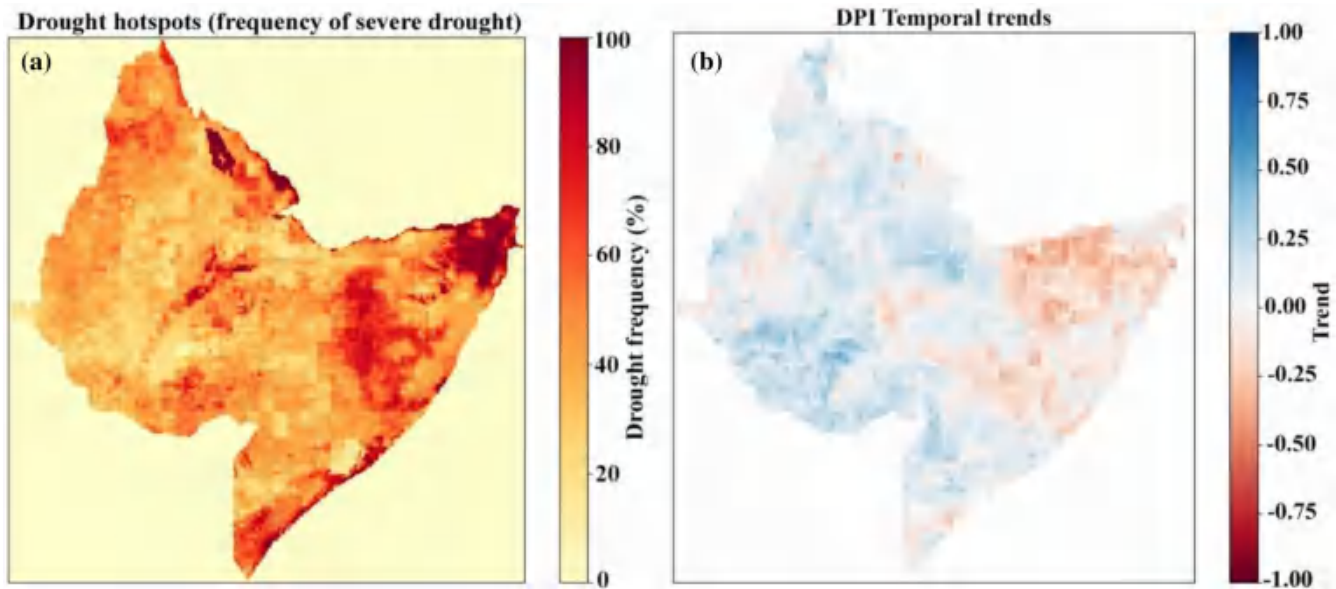


FIGURE 11 | Drought hotspot frequency and DPI temporal trends. (a) Eastern/southeastern HOA face severe droughts 70%–100% of the time. (b) Negative DPI trends (–1 to 0) indicate worsening drought, while northern regions show recovery (positive trends). [Colour figure can be viewed at [wileyonlinelibrary.com](https://onlinelibrary.wiley.com)]

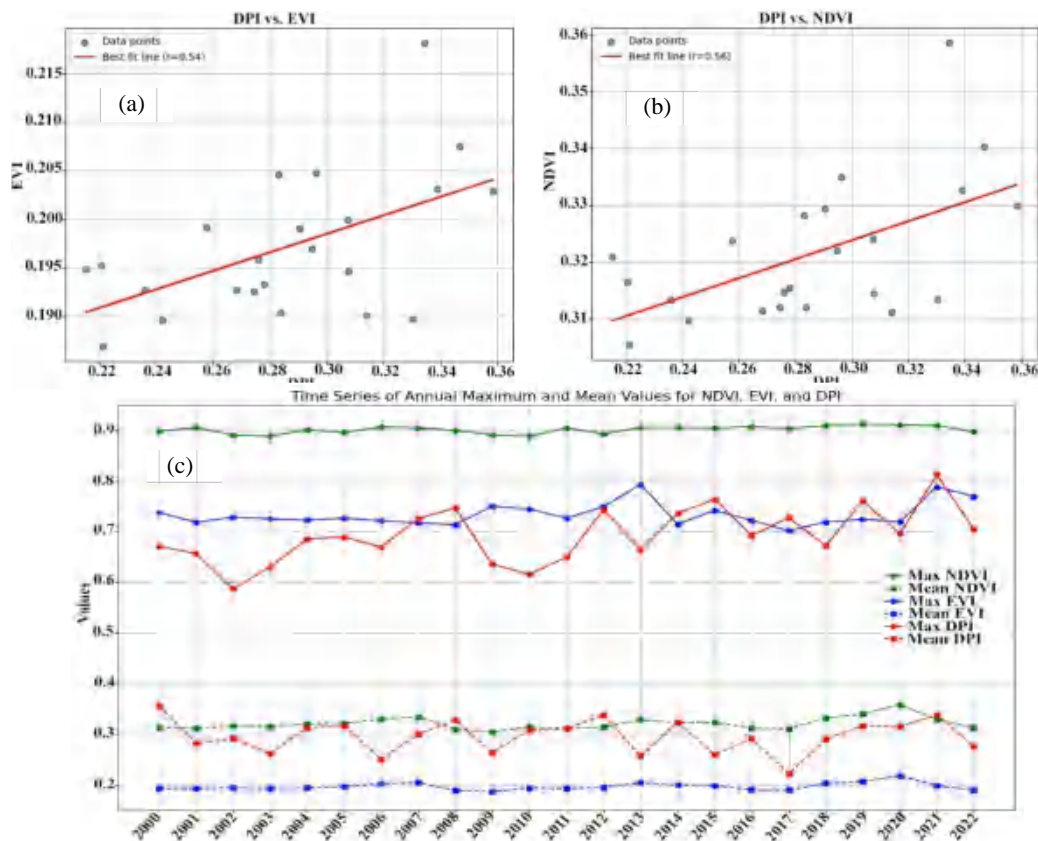


FIGURE 12 | Impact of drought on vegetation health. (a, b) Moderate correlations (NDVI: $r=0.56$; EVI: $r=0.54$) link DPI to vegetation indices. (c) NDVI/EVI declines during droughts (2002, 2015) underscore biomass loss and photosynthetic reduction. [Colour figure can be viewed at [wileyonlinelibrary.com](https://onlinelibrary.wiley.com)]

In Somalia, the harvested area for staple crops, maize—rice, sorghum, sugarcane, sweet potatoes, and wheat—exhibits pronounced interannual variability. During years with low DPI—for

instance, 2004 and 2016—the area harvested for two critical staple crops, maize and sorghum, has been significantly lower. This reflects the direct influence of drought stress on planting

and cultivation activities, where the lack of water and poor soil moisture reduced farmers' potential to use arable land efficiently. A similar pattern is observed in crop production, with maize and sorghum proving most sensitive to drought stress. Their production volumes have been considerably reduced in years with severe droughts, such as 2004 and 2016. In contrast to Somalia, Ethiopia exhibited relatively greater resistance to drought impacts, particularly for maize and sorghum—a noteworthy finding. While this may be partly attributed to a higher prevalence of irrigation in certain agricultural areas of Ethiopia, our study does not include a detailed assessment of irrigation extent or its quantitative impact (Gebul 2021; Haile 2015). Nevertheless, pronounced reductions are observed in years corresponding to drought events, especially for maize, sorghum, and wheat. It is observed that in some low DPI years, that is, 2004 and 2016, huge declines in the area harvested for sorghum and maize were observed, both crops being dependent on rain-fed agriculture. Crop production in Ethiopia follows the same trends seen in the area harvested, including negative anomalies during drought years. Production levels for maize, sorghum, and wheat were substantially lower in drought years (e.g., 2004 and 2016) compared to wet years such as 2008 and 2020.

3.9 | Drought Recovery Time

The concept of drought recovery time is crucial for understanding the resilience of agricultural systems to drought events. In this study, drought recovery time was defined as the period required for the DPI to return to its pre-drought conditions, specifically when DPI values fall below a predefined threshold indicating non-drought or near-normal conditions. This threshold was determined based on the historical distribution of DPI values, with recovery being indicated when DPI returns to within one standard deviation of its long-term mean, indicative of non-stressed conditions.

The average recovery time (in months) during the analysis period exhibited high variability, as illustrated at Figure 13a. Recovery time varies from about 0 months (fast recovery) to over 2 months of delay, with strong peaks in, for example, 2004, 2010, and 2017. These years correspond to the most severe drought events, suggesting that prolonged or intense droughts are associated with extended recovery periods. However, periods of shorter recovery exist in certain years, indicating either relatively mild drought impacts or quite effective recovery mechanisms. The large error bars demonstrate the variability across the different locations within the region, showing the heterogeneity in drought recovery across the landscape. Recovery time also exhibits distinct spatial patterns across the study area, as shown at Figure 13b.

3.10 | Discussion

This study provides a comprehensive and integrated analysis of drought propagation impacts and recovery across the region, hence providing a better understanding of how drought progresses from meteorological to agricultural systems. At the core of the study lies the novel DPI, which serves as a robust tool for quantifying drought severity and its spatiotemporal variability. Combined with other indices like the CSI, SMD, and WDI, it is able to express in detail how the meteorological drought magnitudes are transferred into vegetation stress and agricultural impacts. Moderate positive correlations between DPI and these indices (Table 4) demonstrate the linkage between drought severity and vegetation productivity; during drought years, vegetation greenness, photosynthesis, and canopy structure decline markedly (Rossi et al. 2023).

The spatial analysis identifies key hotspots for drought impacts and variability in recovery times across the HOA (Table 5). Regions such as the eastern lowlands and southeastern HOA

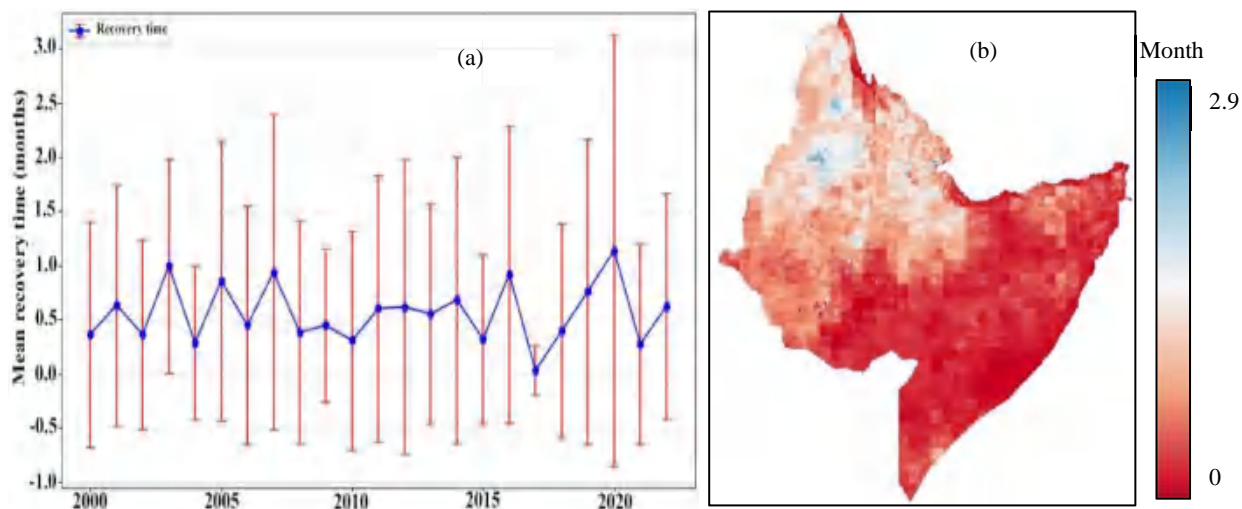


FIGURE 13 | Spatial Distribution of Drought Recovery Time Based on DPI (2000–2022). (a) Mean recovery time, calculated as the number of months for DPI values to return to ≥ 0.8 following drought events. Northern regions, particularly in Ethiopia and Eritrea, exhibit shorter recovery spans (0–2 months), while southeastern zones (e.g., Somalia) show delayed recovery exceeding 2 months. (b) The spatial heterogeneity in recovery time reflects both climatic drivers and ecosystem response capacities. Short recovery times may indicate either quick vegetative response or system fragility due to high exposure and sensitivity. Longer recovery times can signal lower resilience, prolonged biophysical stress, or limited adaptive capacity, particularly in agro-pastoral regions of Somalia. [Colour figure can be viewed at [wileyonlinelibrary.com](https://onlinelibrary.wiley.com/doi/10.1002/joc.7017)]

TABLE 4 | Temporal trends of drought metrics and crop yields (2000–2022).

Year	DPI (drought severity)	Mean NDVI	Max NDVI	Mean EVI	Max EVI	Mean CSI	Mean SMD (mm)	Mean WDI	Maize production (tons)	Sorghum production (tons)	Wheat production (tons)
2000	Severe	0.32	0.58	0.2	0.45	1.8	40.5	−0.75	1,200,000	900,000	1,500,000
2005	Very severe	0.3	0.54	0.18	0.42	1.9	45.3	−0.8	1,000,000	700,000	1,300,000
2010	Moderate	0.35	0.6	0.22	0.48	1.6	30.2	−0.6	1,400,000	950,000	1,600,000
2015	Severe	0.28	0.52	0.16	0.4	1.8	48.7	−0.85	1,050,000	800,000	1,350,000
2022	Mixed	0.34	0.57	0.21	0.46	1.7	35.6	−0.7	1,300,000	900,000	1,500,000

Note: Key drought years (2005, 2015) correlate with NDVI/EVI declines and yield losses (maize: 30%–35% reduction in Somalia). Ethiopia's irrigation moderates impact (e.g., wheat production stability).

TABLE 5 | Spatial variability of drought impacts and recovery.

Region	Mean CSI	Mean SMD (mm)	Mean WDI	Recovery time (months)	Drought hotspot frequency (%)	NDVI (severe drought years)	Crop impact (sensitive crops)
Northern highlands	1.8	45	−0.8	0–2	70–90	Reduced	Maize, Sorghum
Central highlands	1.7	40	−0.75	0–2	50–70	Reduced	Maize, Sorghum
Eastern lowlands	1.9	50	−0.85	8–11	80–100	Severely reduced	Sorghum
Southeastern regions	1.8	48	−0.8	> 4	90–100	Severely reduced	Sorghum
Western forested areas	1.5	35	−0.6	0–2	10–30	Moderately affected	Wheat

Note: Eastern lowlands (Somalia/Afar) face prolonged recovery (> 4 months) and severe vegetation stress. Northern highlands exhibit rapid soil moisture depletion, demanding urgent interventions for rainfed crops.

consistently experienced high drought frequencies of 80%–100% and longer recovery times of > 4 months, reflecting severe drought impacts and limited adaptive capacity (Gebremeskel Haile et al. 2020). The western forested areas showed relatively low frequencies of droughts—10%–30%, indicating stable climatic conditions and greater resilience because of denser vegetation cover. Critically, the analysis of lag times revealed significant regional variability, offering actionable insights for drought monitoring and mitigation. In the northern and central highlands, short lags (0–2 months) reflect rapid soil moisture depletion due to shallow soils and high crop water demand, leaving rainfed agriculture highly vulnerable to abrupt rainfall deficits (Bhardwaj et al. 2020). Conversely, eastern lowlands exhibited prolonged lags (8–11 months), where deeper soils and perennial vegetation (e.g., acacia savannas) delayed agricultural drought onset. Such delays, while temporarily mitigating crop stress, pose risks for pastoral systems reliant on rangelands, as prolonged droughts may exhaust deeper soil moisture, leading to catastrophic vegetation collapse. Furthermore, the lag time between meteorological drought and vegetation response (as captured by NDVI/EVI) highlights ecosystems' capacity to buffer short-term deficits (Epule et al. 2024).

The CSI is instrumental in pinpointing regions where compounded drought stress has prevailed. Generally, high CSI

values in the eastern and southeastern regions indicate prolonged drought conditions, while WDI emphasizes that water availability acts as a primary control on drought impacts (Cagatay et al. 2017).

This suite of indices facilitates the identification of vulnerable regions and provides actionable insights for targeted drought mitigation. DRRI was estimated to quantify the spatial variability in recovery time. It provided the key information about ecosystem resilience (Yao 2022).

It also effectively links drought propagation to agriculture by showing the sensitivity of rainfed systems to drought conditions (Alito and Kerebih 2024; Ayele and Tarekegn 2020). While this study advances the understanding of drought propagation in the HOA, some limitations must be acknowledged. Ground-truthing data were limited in Somalia due to security constraints, necessitating cautious interpretation. Socioeconomic factors, such as irrigation access, population pressure, and adaptive practices, were excluded, potentially oversimplifying drought impact mechanisms. Additionally, the monthly temporal resolution may obscure sub-monthly drought triggers critical for early warning systems.

Our analysis of the relationship between DPI and crop production highlights a significant association. However, it is crucial

to recognize that agricultural production is a complex outcome influenced by a multitude of socio-economic and environmental factors beyond drought. These include, but are not limited to, agricultural input availability (e.g., fertilizers, seeds), market access and prices, conflict, pest and disease outbreaks (e.g., locust infestations), and government policies.

For future research, addressing such factors would enhance the applicability of the findings. Additionally, higher-resolution datasets would enable more refined and localized assessments of drought impacts.

4 | Conclusion

This study assessed drought propagation and impacts across meteorological, hydrological, and agricultural systems, with particular focus on ecosystem recovery dynamics in drought-prone regions. The comprehensive methodology used included the DPI, CSI, SMD, WDI, and DRRI for a robust framework in understanding the drought severity, its cascading impacts, and spatiotemporal variability of recovery. High-resolution climate, soil, and vegetation data from 2000 to 2022 supported the analysis, hence enabling the in-depth analysis of drought hotspots, vegetation stress, agricultural impacts, and recovery patterns.

Results indicate that drought propagation begins with meteorological deficits—precipitation shortages—and subsequently extends to agricultural systems, significantly affecting vegetation health and crop production. Eastern and southeastern areas were identified as critical drought hotspots during most of the investigated time, and severe drought occurred at frequencies of 70%–100%, with worsening trends in those areas. This was blamed on poor precipitation and high rainfed agriculture dependence, raising vulnerabilities. In contrast, northern and northwestern areas showed lower frequencies of drought and trends of improvement, indicating regional variability in the impacts of drought. Delayed propagation (8–11 months) in eastern lowlands underscores the need for early warning systems tailored to rangelands, where subsurface moisture buffers short-term droughts. This study highlights the critical role of lag times (0–11 months) between meteorological drought onset and agricultural impacts. In eastern lowlands, delayed propagation (8–11 months) due to deep soils underscores the need for early warning systems tailored to pastoral systems, whereas rapid lags (0–2 months) in highlands demand urgent interventions for rainfed crops like maize and sorghum. The correlation analysis between DPI and vegetation indices, such as NDVI and EVI, showed a moderate positive relationship, which indicates that with increased drought severity, vegetation greenness, photosynthetic activity, and biomass are negatively affected. This was even more pronounced in drought years, such as 2002, 2005, and 2010, when vegetation health and productivity showed significant declines.

In Somalia, agricultural impacts were severe due to limited water availability and minimal irrigation infrastructure, which constrained staple crop production (e.g., maize and sorghum) during drought years. Ethiopia is relatively better off in terms of agricultural infrastructure but still showed the impacts of severe drought. Furthermore, there was heterogeneity in the recovery

times: longer-term recoveries in the southeast and much faster recoveries in the north.

The study has shown that integrating multiple indices is key to capturing the multi-dimensional nature of drought propagation and impacts. These findings underscore the need for targeted mitigation strategies through irrigation expansion, adoption of drought-resistant crops, and sustainable resource management. Early warning systems in eastern lowlands must account for delayed propagation to provide actionable lead time for pastoral communities reliant on rangelands. This study presents a comprehensive understanding of drought dynamics, thereby establishing a strong foundation for enhancing drought resilience in vulnerable regions.

Author Contributions

Nasser A. M. Abdelrahim: conceptualization, writing – original draft, methodology, validation, visualization, writing – review and editing, software, formal analysis, data curation, resources. **Shuanggen Jin:** investigation, funding acquisition, project administration, supervision, writing – review and editing.

Acknowledgements

The authors would like to thank the editor and reviewers for the constructive comments to improve our manuscript.

Disclosure

The authors have nothing to report.

Conflicts of Interest

The authors declare no conflicts of interest.

Data Availability Statement

The data that support the findings of this study are available in GEE at https://developers.google.com/earth-engine/datasets/catalog/NASA_GLDAS_V021_NOAH_G025_T3H. These data were derived from the following resources available in the public domain: google earth engine, https://developers.google.com/earth-engine/datasets/catalog/NASA_GLDAS_V021_NOAH_G025_T3H.

References

- Abdelrahim, N. A. M., and S. Jin. 2025a. “A Continental-Scale Tracking for Mobile Drought Dynamics Across Africa Using Multivariate Drought Index Fusion.” *International Journal of Applied Earth Observation and Geoinformation* 144: 104917. <https://doi.org/10.1016/j.jag.2025.104917>.
- Abdelrahim, N. A. M., and S. Jin. 2025b. “Genetic Algorithm Optimized Multispectral Soil-Vegetation Drought Index (GA-MSVDI) for Precision Agriculture and Drought Monitoring in North Africa.” *Remote Sensing Applications: Society and Environment* 38: 101603. <https://doi.org/10.1016/j.rsase.2025.101603>.
- Abdelrahim, N. A. M., and S. Jin. 2025c. “A Novel Agricultural Remote Sensing Drought Index (ARSDI) for High-Resolution Drought Assessment in Africa Using Sentinel and Landsat Data.” *Environmental Monitoring and Assessment* 197: 242. <https://doi.org/10.1007/s10661-025-13686-3>.
- Abdelrahim, N. A. M., and S. Jin. 2025d. “Continental Maize Mapping and Distribution in Africa by Integrating Radar and Optical Imagery.”

- Environmental Monitoring and Assessment* 197: 1072. <https://doi.org/10.1007/s10661-025-14502-8>.
- Abera, T. A., J. Heiskanen, P. K. E. Pellikka, and E. E. Maeda. 2020. "Impact of Rainfall Extremes on Energy Exchange and Surface Temperature Anomalies Across Biomes in the Horn of Africa." *Agricultural and Forest Meteorology* 280: 107779. <https://doi.org/10.1016/j.agrformet.2019.107779>.
- Addesso, P., M. Longo, R. Montone, R. Restaino, and G. Vivone. 2017. "Interpolation and Combination Rules for the Temporal and Spatial Enhancement of SEVIRI and MODIS Thermal Image Sequences." *International Journal of Remote Sensing* 38: 1889–1911. <https://doi.org/10.1080/01431161.2017.1283075>.
- Adloff, M., M. B. Singer, D. A. MacLeod, et al. 2022. "Sustained Water Storage in Horn of Africa Drylands Dominated by Seasonal Rainfall Extremes." *Geophysical Research Letters* 49: e2022GL099299. <https://doi.org/10.1029/2022GL099299>.
- Afuecheta, E., and M. H. Omar. 2021. "Characterization of Variability and Trends in Daily Precipitation and Temperature Extremes in the Horn of Africa." *Climate Risk Management* 32: 100295. <https://doi.org/10.1016/j.crm.2021.100295>.
- Agutu, N. O., J. L. Awange, C. Ndehedehe, and M. Mwaniki. 2020. "Consistency of Agricultural Drought Characterization Over Upper Greater Horn of Africa (1982–2013): Topographical, Gauge Density, and Model Forcing Influence." *Science of the Total Environment* 709: 135149. <https://doi.org/10.1016/j.scitotenv.2019.135149>.
- Agutu, N. O., C. E. Ndehedehe, J. L. Awange, F. Kirimi, and M. Mwaniki. 2021. "Understanding Uncertainty of Model-Reanalysis Soil Moisture Within Greater Horn of Africa (1982–2014)." *Journal of Hydrology* 603: 127169. <https://doi.org/10.1016/j.jhydrol.2021.127169>.
- Ahmad, U., A. Alvino, and S. Marino. 2021. "A Review of Crop Water Stress Assessment Using Remote Sensing." *Remote Sensing* 13: 4155. <https://doi.org/10.3390/rs13204155>.
- Akuraju, V. R., D. Ryu, and B. George. 2021. "Estimation of Root-Zone Soil Moisture Using Crop Water Stress Index (CWSI) in Agricultural Fields." *GIScience & Remote Sensing* 58: 340–353. <https://doi.org/10.1080/15481603.2021.1877009>.
- Alasow, A. A., M. M. Hamed, M. Rady, M. A. Arab, M. K. I. Muhammad, and S. Shahid. 2024. "Spatiotemporal Analysis of Soil Moisture Drought in the Horn of Africa." *Theoretical and Applied Climatology* 155: 7165–7176. <https://doi.org/10.1007/s00704-024-05052-z>.
- Alito, K. T., and M. S. Kerebih. 2024. "Spatio-Temporal Assessment of Agricultural Drought Using Remote Sensing and Ground-Based Data Indices in the Northern Ethiopian Highland." *Journal of Hydrology: Regional Studies* 52: 101700. <https://doi.org/10.1016/j.ejrh.2024.101700>.
- Alordzinu, K. E., J. Li, Y. Lan, S. A. Appiah, A. Al Aasmi, and H. Wang. 2021. "Rapid Estimation of Crop Water Stress Index on Tomato Growth." *Sensors (Basel)* 21: 5142. <https://doi.org/10.3390/s21155142>.
- Amazirh, A., A. Chehbouni, E. H. Bouras, M. Benkirane, B. A. Hssaine, and D. Entekhabi. 2023. "Drought Cascade Lag Time Estimation Across Africa Based on Remote Sensing of Hydrological Cycle Components." *Advances in Water Resources* 182: 104586. <https://doi.org/10.1016/j.advwatres.2023.104586>.
- Ayele, A., and K. Tarekegn. 2020. "The Impact of Urbanization Expansion on Agricultural Land in Ethiopia: A Review." *Environmental & Socio-Economic Studies* 8: 73–80. <https://doi.org/10.2478/enviro-2020-0024>.
- Beyene, T. K., A. Agarwal, M. K. Jain, and B. K. Yadav. 2023. "Investigation of the Propagation of Meteorological to Hydrological Drought and Water Required to Recover From Drought Over Ethiopian Basins." *Journal of Water and Climate Change* 14: 2988–3009. <https://doi.org/10.2166/wcc.2023.024>.
- Bhanja, S. N., A. Mukherjee, D. Saha, I. Velicogna, and J. S. Famiglietti. 2016. "Validation of GRACE Based Groundwater Storage Anomaly Using In-Situ Groundwater Level Measurements in India." *Journal of Hydrology* 543: 729–738. <https://doi.org/10.1016/j.jhydrol.2016.10.042>.
- Bhardwaj, K., D. Shah, S. Aadhar, and V. Mishra. 2020. "Propagation of Meteorological to Hydrological Droughts in India." *JGR-Atmospheres* 125: e2020JD033455. <https://doi.org/10.1029/2020JD033455>.
- Bhatti, H., T. Rientjes, A. Haile, E. Habib, and W. Verhoef. 2016. "Evaluation of Bias Correction Method for Satellite-Based Rainfall Data." *Sensors (Basel)* 16: 884. <https://doi.org/10.3390/s16060884>.
- Bilal, S. B., and V. Gupta. 2024. "Deciphering the Spatial Fingerprint of Drought Propagation Through Precipitation, Vegetation and Groundwater." *International Journal of Climatology* 44: 4443–4461. <https://doi.org/10.1002/joc.8590>.
- Bussalleu, A., G. Hoek, I. Kloog, N. Probst-Hensch, M. Rössli, and K. De Hoogh. 2024. "Modelling Europe-Wide Fine Resolution Daily Ambient Temperature for 2003–2020 Using Machine Learning." *Science of the Total Environment* 928: 172454. <https://doi.org/10.1016/j.scitotenv.2024.172454>.
- Cagatay, T., A. Atilgan, D. Hasan, and A. Adil. 2017. "Comparation of Crop Water Stress Index (CWSI) and Water Deficit Index (WDI) by Using Remote Sensing (RS)." *Infrastruktura i Ekologia Terenów Wiejskich/Infrastructure and Ecology of Rural Areas* 3: 879–894. <https://doi.org/10.14597/infraeco.2017.3.1.068>.
- Cao, M. 2022. "Assessing the Performance of Satellite Soil Moisture on Agricultural Drought Monitoring in the North China Plain." *Agricultural Water Management* 263: 107450.
- Chaulagain, S., M. Lamichhane, U. Chaulagain, S. Gyawali, S. Shrestha, and V. P. Pandey. 2025. "Evaluating Different Drought Products for Assessing Drought and Implications on Agriculture in Nepal." *Results in Engineering* 25: 104205. <https://doi.org/10.1016/j.rineng.2025.104205>.
- Das, S., J. Das, and N. V. Umamahesh. 2022. "Investigating the Propagation of Droughts Under the Influence of Large-Scale Climate Indices in India." *Journal of Hydrology* 610: 127900. <https://doi.org/10.1016/j.jhydrol.2022.127900>.
- Das, S., J. Das, and N. V. Umamahesh. 2023. "A Non-Stationary Based Approach to Understand the Propagation of Meteorological to Agricultural Droughts." *Water Resources Management* 37: 2483–2504. <https://doi.org/10.1007/s11269-022-03297-9>.
- De Sousa, L. M., L. Poggio, N. H. Batjes, et al. 2020. "SoilGrids 2.0: Producing Quality-Assessed Soil Information for Theglobe." <https://doi.org/10.5194/soil-2020-65>.
- Ding, Y., X. Gong, Z. Xing, et al. 2021. "Attribution of Meteorological, Hydrological and Agricultural Drought Propagation in Different Climatic Regions of China." *Agricultural Water Management* 255: 106996. <https://doi.org/10.1016/j.agwat.2021.106996>.
- Dong, J., L. Xing, N. Cui, L. Zhao, L. Guo, and D. Gong. 2023. "Standardized Precipitation Evapotranspiration Index (SPEI) Estimated Using Variant Long Short-Term Memory Network at Four Climatic Zones of China." *Computers and Electronics in Agriculture* 213: 108253. <https://doi.org/10.1016/j.compag.2023.108253>.
- Edokossi, K., S. Jin, A. Calabia, I. Molina, and U. Mazhar. 2024. "Evaluation of SMAP and CYGNSS Soil Moistures in Drought Prediction Using Multiple Linear Regression and GLDAS Product." *Photogrammetric Engineering & Remote Sensing* 90: 303–312.
- Elameen, A. M., S. Jin, and D. Olago. 2023. "Identification of Drought Events in Major Basins of Africa From GRACE Total Water Storage and Modeled Products." *Photogrammetric Engineering & Remote Sensing* 89: 221–232.
- Elnashar, A., L. Wang, B. Wu, W. Zhu, and H. Zeng. 2021. "Synthesis of Global Actual Evapotranspiration From 1982 to 2019." *Earth System Science Data* 13: 447–480. <https://doi.org/10.5194/essd-13-447-2021>.

- Epule, T. E., A. Chehbouni, D. Dhiba, and E. L. Molua. 2024. "A Regional Stocktake of Maize Yield Vulnerability to Droughts in the Horn of Africa." *Environmental Monitoring and Assessment* 196: 76. <https://doi.org/10.1007/s10661-023-12229-y>.
- Faiz, M. A., Y. Zhang, X. Tian, et al. 2023. "Time Series Analysis for Droughts Characteristics Response to Propagation." *International Journal of Climatology* 43: 1561–1575. <https://doi.org/10.1002/joc.7933>.
- FAO. 2019. "The State of Food Security and Nutrition in the World 2019: Safeguarding Against Economic Slowdowns and Downturns." In *The State of Food Security and Nutrition in the World Series*, 1st ed. United Nations Publications.
- FAO. 2021. "A Rapid Review of Drought Risk Mitigation Measures." FAO. <https://doi.org/10.4060/cb7085en>.
- FAO. 2022. "Drought in the Horn of Africa – Rapid Response and Mitigation Plan to Avert a Humanitarian Catastrophe." FAO. <https://doi.org/10.4060/cb8280en>.
- Farrag, F. A., Y. G. Mostafa, and N. A. Mohamed. 2020. "Detecting Land Cover Changes Using VHR Satellite Images: A Comparative Study." *Journal of Engineering Sciences* 48: 200–211. <https://doi.org/10.21608/jesaun.2019.264927>.
- Fawen, L., Z. Manjing, Z. Yong, and J. Rengui. 2023. "Influence of Irrigation and Groundwater on the Propagation of Meteorological Drought to Agricultural Drought." *Agricultural Water Management* 277: 108099. <https://doi.org/10.1016/j.agwat.2022.108099>.
- García, S., S. Ramírez-Gallego, J. Luengo, J. M. Benítez, and F. Herrera. 2016. "Big Data Preprocessing: Methods and Prospects." *Big Data Analytics* 1: 9. <https://doi.org/10.1186/s41044-016-0014-0>.
- Ge, C., P. Sun, R. Yao, Y. Zhang, H. Shen, and H. Yang. 2025. "Drivers of Ecological Drought Recovery: Insights From Meteorological and Soil Drought Impact." *Journal of Hydrology* 646: 132324. <https://doi.org/10.1016/j.jhydrol.2024.132324>.
- Gebremeskel Haile, G., Q. Tang, G. Leng, et al. 2020. "Long-Term Spatiotemporal Variation of Drought Patterns Over the Greater Horn of Africa." *Science of the Total Environment* 704: 135299. <https://doi.org/10.1016/j.scitotenv.2019.135299>.
- Gebul, M. A. 2021. "Trend, Status, and Challenges of Irrigation Development in Ethiopia—A Review." *Sustainability* 13: 5646. <https://doi.org/10.3390/su13105646>.
- Gevaert, A. I., T. I. E. Veldkamp, and P. J. Ward. 2018. "The Effect of Climate Type on Timescales of Drought Propagation in an Ensemble of Global Hydrological Models." *Hydrology and Earth System Sciences* 22: 4649–4665. <https://doi.org/10.5194/hess-22-4649-2018>.
- Guga, S., Y. Ma, D. Riao, F. Zhi, J. Xu, and J. Zhang. 2023. "Drought Monitoring of Sugarcane and Dynamic Variation Characteristics Under Global Warming: A Case Study of Guangxi, China." *Agricultural Water Management* 275: 108035. <https://doi.org/10.1016/j.agwat.2022.108035>.
- Guiqin, J., Y. Fuliang, and Z. Yong. 2012. "An Analysis of Vulnerability to Agricultural Drought in China Using the Expand Grey Relation Analysis Method." *Procedia Engineering* 28: 670–676. <https://doi.org/10.1016/j.proeng.2012.01.789>.
- Haile, G. G. 2015. "Irrigation in Ethiopia, a Review."
- Han, X., Y. Li, W. Yu, and L. Feng. 2022. "Attribution of the Extreme Drought in the Horn of Africa During Short-Rains of 2016 and Long-Rains of 2017." *Water* 14: 409. <https://doi.org/10.3390/w14030409>.
- Han, Z., S. Huang, Q. Huang, et al. 2019. "Propagation Dynamics From Meteorological to Groundwater Drought and Their Possible Influence Factors." *Journal of Hydrology* 578: 124102. <https://doi.org/10.1016/j.jhydrol.2019.124102>.
- Hao, Y., J. Baik, S. Fred, and M. Choi. 2022. "Comparative Analysis of Two Drought Indices in the Calculation of Drought Recovery Time and Implications on Drought Assessment: East Africa's Lake Victoria Basin." *Stochastic Environmental Research and Risk Assessment* 36: 1943–1958. <https://doi.org/10.1007/s00477-021-02137-3>.
- Hengl, T., J. Mendes De Jesus, G. B. M. Heuvelink, et al. 2017. "SoilGrids250m: Global Gridded Soil Information Based on Machine Learning." *PLoS One* 12: e0169748. <https://doi.org/10.1371/journal.pone.0169748>.
- Ho, S., L. Tian, M. Disse, and Y. Tuo. 2021. "A New Approach to Quantify Propagation Time From Meteorological to Hydrological Drought." *Journal of Hydrology* 603: 127056. <https://doi.org/10.1016/j.jhydrol.2021.127056>.
- Iman Bin Hussain, M. D., V. Katiyar, M. Nagai, and D. Ichikawa. 2025. "Enhancing Satellite Image Coregistration Using Mirror Array as Artificial Point Source for Multisource Image Harmonization." *IEEE Journal of Selected Topics in Applied Earth Observations and Remote Sensing* 18: 16983–16996. <https://doi.org/10.1109/JSTARS.2025.3582238>.
- Inocencio, T. d. M., A. R. Neto, M. Oertel, F. J. Meza, and C. A. Scott. 2021. "Linking Drought Propagation With Episodes of Climate-Induced Water Insecurity in Pernambuco State – Northeast Brazil." *Journal of Arid Environments* 193: 104593.
- Jehanzaib, M., M. N. Sattar, J.-H. Lee, and T.-W. Kim. 2020. "Investigating Effect of Climate Change on Drought Propagation From Meteorological to Hydrological Drought Using Multi-Model Ensemble Projections." *Stochastic Environmental Research and Risk Assessment* 34: 7–21. <https://doi.org/10.1007/s00477-019-01760-5>.
- Jeong, M.-S., S.-Y. Park, Y.-J. Kim, H.-C. Yoon, and J.-H. Lee. 2024. "Identification of Propagation Characteristics From Meteorological Drought to Hydrological Drought Using Daily Drought Indices and Lagged Correlations Analysis." *Journal of Hydrology: Regional Studies* 55: 101939. <https://doi.org/10.1016/j.ejrh.2024.101939>.
- Jin, S., A. Camps, Y. Jia, et al. 2024. "Remote Sensing and Its Applications Using GNSS Reflected Signals: Advances and Prospects." *Satellite Navigation* 5: 19. <https://doi.org/10.1186/s43020-024-00139-4>.
- Jin, S., and T. Zhang. 2016. "Terrestrial Water Storage Anomalies Associated With Drought in Southwestern USA From GPS Observations." *Surveys in Geophysics* 37: 1139–1156. <https://doi.org/10.1007/s10712-016-9385-z>.
- Joordens, J. C. A., C. S. Feibel, H. B. Vonhof, A. S. Schulp, and D. Kroon. 2019. "Relevance of the Eastern African Coastal Forest for Early Hominin Biogeography." *Journal of Human Evolution* 131: 176–202. <https://doi.org/10.1016/j.jhevol.2019.03.012>.
- Jury, M. R. 2023. "Characterizing Northeast Africa Drought and Its Drivers." *Climate* 11: 130. <https://doi.org/10.3390/cli11060130>.
- Kafy, A.-A., A. Bakshi, M. Saha, et al. 2023. "Assessment and Prediction of Index Based Agricultural Drought Vulnerability Using Machine Learning Algorithms." *Science of the Total Environment* 867: 161394. <https://doi.org/10.1016/j.scitotenv.2023.161394>.
- Katimbo, A., D. R. Rudnick, K. C. DeJonge, et al. 2022. "Crop Water Stress Index Computation Approaches and Their Sensitivity to Soil Water Dynamics." *Agricultural Water Management* 266: 107575. <https://doi.org/10.1016/j.agwat.2022.107575>.
- Khan, M. I., X. Zhu, X. Jiang, et al. 2021. "Projection of Future Drought Characteristics Under Multiple Drought Indices." *Water (Basel)* 13: 1238. <https://doi.org/10.3390/w13091238>.
- Kogan, F., W. Guo, and W. Yang. 2019. "Drought and Food Security Prediction From NOAA New Generation of Operational Satellites." *Geomatics, Natural Hazards and Risk* 10: 651–666. <https://doi.org/10.1080/19475705.2018.1541257>.

- Leal Filho, W., I. Djekic, S. Smetana, and M. Kovaleva, eds. 2022. *Handbook of Climate Change Across the Food Supply Chain, Climate Change Management*. Springer International Publishing. <https://doi.org/10.1007/978-3-030-87934-1>.
- Li, J. 2024. "A Novel Composite Drought Index Combining Precipitation, Temperature and Evapotranspiration Used for Drought Monitoring in the Huang-Huai-Hai Plain." *Agricultural Water Management* 291: 108626.
- Li, P., L. Jia, J. Lu, M. Jiang, C. Zheng, and M. Menenti. 2024. "Investigating the Response of Vegetation to Flash Droughts by Using Cross-Spectral Analysis and an Evapotranspiration-Based Drought Index." *Remote Sensing* 16: 1564. <https://doi.org/10.3390/rs16091564>.
- Li, R., N. Chen, X. Zhang, et al. 2020. "Quantitative Analysis of Agricultural Drought Propagation Process in the Yangtze River Basin by Using Cross Wavelet Analysis and Spatial Autocorrelation." *Agricultural and Forest Meteorology* 280: 107809. <https://doi.org/10.1016/j.agrformet.2019.107809>.
- Li, Y., S. Huang, H. Wang, et al. 2022. "High-Resolution Propagation Time From Meteorological to Agricultural Drought at Multiple Levels and Spatiotemporal Scales." *Agricultural Water Management* 262: 107428. <https://doi.org/10.1016/j.agwat.2021.107428>.
- Liu, X., X. Zhu, Y. Pan, S. Li, Y. Liu, and Y. Ma. 2016. "Agricultural Drought Monitoring: Progress, Challenges, and Prospects." *Journal of Geographical Sciences* 26: 750–767. <https://doi.org/10.1007/s11442-016-1297-9>.
- Ma, F., X. Yuan, and X. Liu. 2023. "Intensification of Drought Propagation Over the Yangtze River Basin Under Climate Warming." *International Journal of Climatology* 43: 5640–5661. <https://doi.org/10.1002/joc.8165>.
- Ma, Y., J. Ren, S. Kang, J. Niu, and L. Tong. 2025. "Spatial-Temporal Dynamics of Meteorological and Agricultural Drought in Northwest China: Propagation, Drivers and Prediction." *Journal of Hydrology* 650: 132492. <https://doi.org/10.1016/j.jhydrol.2024.132492>.
- Mahmood, T., J. Löw, J. Pöhlitz, J. L. Wenzel, and C. Conrad. 2024. "Estimation of 100 m Root Zone Soil Moisture by Downscaling 1 Km Soil Water Index With Machine Learning and Multiple Geodata." *Environmental Monitoring and Assessment* 196: 823. <https://doi.org/10.1007/s10661-024-12969-5>.
- Masih, I., S. Maskey, F. E. F. Mussá, and P. Trambauer. 2014. "A Review of Droughts on the African Continent: A Geospatial and Long-Term Perspective." *Hydrology and Earth System Sciences* 18: 3635–3649. <https://doi.org/10.5194/hess-18-3635-2014>.
- Measho, S., B. Chen, P. Pellikka, et al. 2020. "Land Use/Land Cover Changes and Associated Impacts on Water Yield Availability and Variations in the Mereb-Gash River Basin in the Horn of Africa." *JGR Biogeosciences* 125: e2020JG005632. <https://doi.org/10.1029/2020JG005632>.
- Mehravar, S., M. Amani, A. Moghimi, et al. 2021. "Temperature-Vegetation-Soil Moisture-Precipitation Drought Index (TVMPDI); 21-Year Drought Monitoring in Iran Using Satellite Imagery Within Google Earth Engine." *Advances in Space Research* 68: 4573–4593. <https://doi.org/10.1016/j.asr.2021.08.041>.
- Mohseni, F., A. Ahrari, J.-H. Haunert, and C. Montzka. 2024. "The Synergies of SMAP Enhanced and MODIS Products in a Random Forest Regression for Estimating 1 Km Soil Moisture Over Africa Using Google Earth Engine." *Big Earth Data* 8: 33–57. <https://doi.org/10.1080/20964471.2023.2257905>.
- Mullissa, A., A. Vollrath, C. Odongo-Braun, et al. 2021. "Sentinel-1 SAR Backscatter Analysis Ready Data Preparation in Google Earth Engine." *Remote Sensing* 13: 1954. <https://doi.org/10.3390/rs13101954>.
- Mwangi, E., F. Wetterhall, E. Dutra, F. Di Giuseppe, and F. Pappenberger. 2013. "Forecasting Droughts in East Africa." <https://doi.org/10.5194/hessd-10-10209-2013>.
- Naumann, G., P. Barbosa, L. Garrote, A. Iglesias, and J. Vogt. 2014. "Exploring Drought Vulnerability in Africa: An Indicator Based Analysis to Be Used in Early Warning Systems." *Hydrology and Earth System Sciences* 18: 1591–1604. <https://doi.org/10.5194/hess-18-1591-2014>.
- Naumann, G., E. Dutra, P. Barbosa, F. Pappenberger, F. Wetterhall, and J. V. Vogt. 2014. "Comparison of Drought Indicators Derived From Multiple Data Sets Over Africa." *Hydrology and Earth System Sciences* 18: 1625–1640.
- Nguvava, M., and B. J. Abiodun. 2023. "Potential Impacts of 1.5°C and 2°C Global Warming Levels on Drought Modes Over Eastern Africa." *Climatic Change* 176: 163. <https://doi.org/10.1007/s10584-023-03631-z>.
- Nguyen, H., M. C. Wheeler, J. A. Otkin, T. Nguyen-Huy, and T. Cowan. 2023. "Climatology and Composite Evolution of Flash Drought Over Australia and Its Vegetation Impacts." *Journal of Hydrometeorology* 24: 1087–1101. <https://doi.org/10.1175/JHM-D-22-0033.1>.
- Nigatu, Z. M., W. You, and A. M. Melesse. 2024. "Drought Dynamics in the Nile River Basin: Meteorological, Agricultural, and Groundwater Drought Propagation." *Remote Sensing* 16: 919.
- Ning, S., M. Zhang, X. Xu, et al. 2025. "Spatiotemporal Propagation of Compound Drought Events in China: An Approach Combining 3D Clustering and Daily-Scale Extended Convergent Cross Mapping." <https://doi.org/10.2139/ssrn.5127582>.
- Odongo, R. A., H. De Moel, and A. F. Van Loon. 2023. "Propagation From Meteorological to Hydrological Drought in the Horn of Africa Using Both Standardized and Threshold-Based Indices." *Natural Hazards and Earth System Sciences* 23: 2365–2386. <https://doi.org/10.5194/nhess-23-2365-2023>.
- Ogunrinde, A. T., P. Adigun, X. Xian, et al. 2024. "Multi-Scale Drought Variability Over West Africa and the Associated Large-Scale Circulation Patterns." *Geomatics, Natural Hazards and Risk* 15: 2409199. <https://doi.org/10.1080/19475705.2024.2409199>.
- Ouatiki, H., A. Boudhar, and A. Chehbouni. 2023. "Accuracy Assessment and Bias Correction of Remote Sensing-Based Rainfall Products Over Semiarid Watersheds." *Theoretical and Applied Climatology* 154: 763–780. <https://doi.org/10.1007/s00704-023-04586-y>.
- Pan, Z., S. Yang, X. Ren, et al. 2023. "GEE Can Prominently Reduce Uncertainties From Input Data and Parameters of the Remote Sensing-Driven Distributed Hydrological Model." *Science of the Total Environment* 870: 161852. <https://doi.org/10.1016/j.scitotenv.2023.161852>.
- Pandey, P., K. K. Dewangan, and D. K. Dewangan. 2017. "Enhancing the Quality of Satellite Images by Preprocessing and Contrast Enhancement." In Presented at the 2017 International Conference on Communication and Signal Processing (ICCCSP), IEEE, Chennai, pp. 0056–0060. <https://doi.org/10.1109/ICCCSP.2017.8286525>.
- Pastick, N. J., B. K. Wylie, and Z. Wu. 2018. "Spatiotemporal Analysis of Landsat-8 and Sentinel-2 Data to Support Monitoring of Dryland Ecosystems." *Remote Sensing* 10: 791. <https://doi.org/10.3390/rs10050791>.
- Poggio, L., L. M. De Sousa, N. H. Batjes, et al. 2021. "SoilGrids 2.0: Producing Soil Information for the Globe With Quantified Spatial Uncertainty." *Soil* 7: 217–240. <https://doi.org/10.5194/soil-7-217-2021>.
- Qu, C., X. Hao, and J. J. Qu. 2019. "Monitoring Extreme Agricultural Drought Over the Horn of Africa (HOA) Using Remote Sensing Measurements." *Remote Sensing* 11: 902. <https://doi.org/10.3390/rs11080902>.
- Rincón-Avalos, P., A. Khouakhi, O. Mendoza-Cano, and K. M. Paredes-Bonilla. 2022. "Evaluation of Satellite Precipitation Products Over Mexico Using Google Earth Engine." *Journal of Hydroinformatics* 24: 711–729.
- Rossi, J. B., A. Ruhoff, A. S. Fleischmann, and L. Laipelt. 2023. "Drought Propagation in Brazilian Biomes Revealed by Remote Sensing." *Remote Sensing* 15: 454. <https://doi.org/10.3390/rs15020454>.

- Sahaar, S. A., and J. D. Niemann. 2024. "Estimating Rootzone Soil Moisture by Fusing Multiple Remote Sensing Products With Machine Learning." *Remote Sensing* 16: 3699. <https://doi.org/10.3390/rs16193699>.
- Sakellariou, S., M. Spiliotopoulos, N. Alpanakis, et al. 2024. "Spatiotemporal Drought Assessment Based on Gridded Standardized Precipitation Index (SPI) in Vulnerable Agroecosystems." *Sustainability* 16: 1240. <https://doi.org/10.3390/su16031240>.
- Sardooi, E. R., A. Azareh, H. E. Damaneh, and H. E. Damaneh. 2021. "Drought Monitoring Using MODIS Land Surface Temperature and Normalized Difference Vegetation Index Products in Semi-Arid Areas of Iran." *Journal of Rangeland Science* 11: 402–418.
- Sazib, N., I. Mladenova, and J. Bolten. 2018. "Leveraging the Google Earth Engine for Drought Assessment Using Global Soil Moisture Data." *Remote Sensing* 10: 1265. <https://doi.org/10.3390/rs10081265>.
- Senay, G. B., M. Friedrichs, C. Morton, et al. 2022. "Mapping Actual Evapotranspiration Using Landsat for the Conterminous United States: Google Earth Engine Implementation and Assessment of the SSEBop Model." *Remote Sensing of Environment* 275: 113011. <https://doi.org/10.1016/j.rse.2022.113011>.
- Shao, G., W. Han, H. Zhang, et al. 2021. "Mapping Maize Crop Coefficient Kc Using Random Forest Algorithm Based on Leaf Area Index and UAV-Based Multispectral Vegetation Indices." *Agricultural Water Management* 252: 106906. <https://doi.org/10.1016/j.agwat.2021.106906>.
- Shen, R., A. Huang, B. Li, and J. Guo. 2019. "Construction of a Drought Monitoring Model Using Deep Learning Based on Multi-Source Remote Sensing Data." *International Journal of Applied Earth Observation and Geoinformation* 79: 48–57. <https://doi.org/10.1016/j.jag.2019.03.006>.
- Tierney, J. E., C. C. Ummenhofer, and P. B. deMenocal. 2015. "Past and Future Rainfall in the Horn of Africa." *Science Advances* 1: e1500682. <https://doi.org/10.1126/sciadv.1500682>.
- Todmal, R. S. 2024. "Intensity, Frequency and Coverage of Hydro-Meteorological Droughts and Agriculture in the Semi-Arid Basins of Maharashtra (India)." *Climatic Change* 177: 140. <https://doi.org/10.1007/s10584-024-03794-3>.
- Venkatappa, M., N. Sasaki, P. Han, and I. Abe. 2021. "Impacts of Droughts and Floods on Croplands and Crop Production in Southeast Asia – An Application of Google Earth Engine." *Science of the Total Environment* 795: 148829. <https://doi.org/10.1016/j.scitotenv.2021.148829>.
- Vicente-Serrano, S. M., S. Beguería, and J. I. López-Moreno. 2010. "A Multiscalar Drought Index Sensitive to Global Warming: The Standardized Precipitation Evapotranspiration Index." *Journal of Climate* 23: 1696–1718. <https://doi.org/10.1175/2009JCLI2909.1>.
- Warsame, A. A., I. A. Sheik-Ali, A. O. Ali, and S. A. Sarkodie. 2021. "Climate Change and Crop Production Nexus in Somalia: An Empirical Evidence From ARDL Technique." *Environmental Science and Pollution Research* 28: 19838–19850. <https://doi.org/10.1007/s11356-020-11739-3>.
- Wei, W., T. Liu, L. Zhou, et al. 2023. "Drought-Related Spatiotemporal Cumulative and Time-Lag Effects on Terrestrial Vegetation Across China." *Remote Sensing* 15: 4362. <https://doi.org/10.3390/rs15184362>.
- Wei, W., J. Zhang, L. Zhou, B. Xie, J. Zhou, and C. Li. 2021. "Comparative Evaluation of Drought Indices for Monitoring Drought Based on Remote Sensing Data." *Environmental Science and Pollution Research* 28: 20408–20425. <https://doi.org/10.1007/s11356-020-12120-0>.
- Wen, Y., L. Zhou, L. Kang, H. Chen, and J. Guo. 2023. "Drought Risk Analysis Based on Multivariate Copula Function in Henan Province, China." *Geomatics, Natural Hazards and Risk* 14: 2223344. <https://doi.org/10.1080/19475705.2023.2223344>.
- Wilhelmi, O. V., and D. A. Wilhite. 2002. "Assessing Vulnerability to Agricultural Drought: A Nebraska Case Study." *Natural Hazards* 25: 37–58.
- Wu, C., Y. Xu, J. Jin, et al. 2024. "Meteorological to Agricultural Drought Propagation Time Analysis and Driving Factors Recognition Considering Time-Variant Characteristics." *Water Resources Management* 38: 991–1010. <https://doi.org/10.1007/s11269-023-03705-8>.
- Wu, W., Y. Li, X. Luo, Y. Zhang, X. Ji, and X. Li. 2019. "Performance Evaluation of the CHIRPS Precipitation Dataset and Its Utility in Drought Monitoring Over Yunnan Province, China." *Geomatics, Natural Hazards and Risk* 10: 2145–2162. <https://doi.org/10.1080/19475705.2019.1683082>.
- Xiang, K., Y. Li, R. Horton, and H. Feng. 2020. "Similarity and Difference of Potential Evapotranspiration and Reference Crop Evapotranspiration – A Review." *Agricultural Water Management* 232: 106043. <https://doi.org/10.1016/j.agwat.2020.106043>.
- Xu, Y., X. Zhang, Z. Hao, V. P. Singh, and F. Hao. 2021. "Characterization of Agricultural Drought Propagation Over China Based on Bivariate Probabilistic Quantification." *Journal of Hydrology* 598: 126194. <https://doi.org/10.1016/j.jhydrol.2021.126194>.
- Xu, Z., Z. Wu, Q. Shao, H. He, and X. Guo. 2023. "From Meteorological to Agricultural Drought: Propagation Time and Probabilistic Linkages." *Journal of Hydrology: Regional Studies* 46: 101329. <https://doi.org/10.1016/j.ejrh.2023.101329>.
- Yao, Y. 2022. "Evaluation of Ecosystem Resilience to Drought Based on Drought Intensity and Recovery Time." *Agricultural and Forest Meteorology* 314: 108809.
- Yaswanth, P., B. A. M. Kannan, V. M. Bindhu, C. Balaji, and B. Narasimhan. 2023. "Evaluation of Remote Sensing Rainfall Products, Bias Correction and Temporal Disaggregation Approaches, for Improved Accuracy in Hydrologic Simulations." *Water Resources Management* 37: 3069–3092. <https://doi.org/10.1007/s11269-023-03486-0>.
- You, Y., Y. Zhang, Y. Lu, Y. Hao, Z. Tang, and H. Hou. 2025. "Spatiotemporal Dynamics of Drought in the Huai River Basin (2012–2018): Analyzing Patterns Through Hydrological Simulation and Geospatial Methods." *Remote Sensing* 17: 241. <https://doi.org/10.3390/rs17020241>.
- Zhang, H., F. Huang, X. Hong, and P. Wang. 2022. "A Sensor Bias Correction Method for Reducing the Uncertainty in the Spatiotemporal Fusion of Remote Sensing Images." *Remote Sensing* 14: 3274. <https://doi.org/10.3390/rs14143274>.
- Zhen, Z., S. Chen, T. Yin, and J.-P. Gastellu-Etchegorry. 2023. "Globally Quantitative Analysis of the Impact of Atmosphere and Spectral Response Function on 2-Band Enhanced Vegetation Index (EVI2) Over Sentinel-2 and Landsat-8." *ISPRS Journal of Photogrammetry and Remote Sensing* 205: 206–226. <https://doi.org/10.1016/j.isprsjprs.2023.09.024>.
- Zhou, Z., P. Wang, L. Li, et al. 2024. "Recent Development on Drought Propagation: A Comprehensive Review." *Journal of Hydrology* 645: 132196. <https://doi.org/10.1016/j.jhydrol.2024.132196>.
- Zomer, R. J., J. Xu, and A. Trabucco. 2022. "Version 3 of the Global Aridity Index and Potential Evapotranspiration Database." *Scientific Data* 9: 409. <https://doi.org/10.1038/s41597-022-01493-1>.